

NASA Technical Paper 1188

0134545



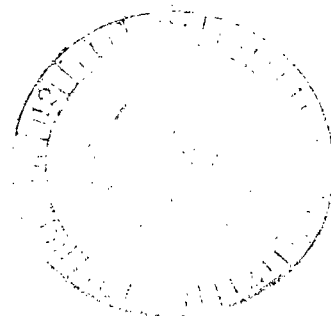
LOAN COPY: RET
AFWL TECHNICAL
KIRTLAND AFB, I

Experimental and Analytical Investigation of a Nonaxisymmetric Wedge Nozzle at Static Conditions

George T. Carson, Jr., and Mary L. Mason

JULY 1978

NASA





NASA Technical Paper 1188

Experimental and Analytical Investigation of a Nonaxisymmetric Wedge Nozzle at Static Conditions

George T. Carson, Jr., and Mary L. Mason
Langley Research Center
Hampton, Virginia



National Aeronautics
and Space Administration

**Scientific and Technical
Information Office**

1978

SUMMARY

An experimental investigation of a nonaxisymmetric wedge nozzle has been conducted at static conditions. The resulting data, in the form of detailed pressure distributions and oil flow photographs, expand the current nonaxisymmetric nozzle data base. For the range of nozzle pressure ratios in this experiment, the nozzle exhaust flow exhibits regions of predominately two-dimensional flow and regions of highly three-dimensional flow, characterized by shock waves and vortex flow.

An analytical investigation has been conducted to evaluate a two-dimensional, inviscid, time-dependent theory as a nonaxisymmetric nozzle performance predictor. Results indicate good agreement between theory and experiment in regions of predominately two-dimensional flow for all nozzle pressure ratios considered. Agreement is considerably weaker in the regions of three-dimensional flow, especially at the higher nozzle pressure ratios. When three-dimensional effects are minimized by the flow characteristics, the agreement between theory and experiment improves; agreement remains optimal at the lower nozzle pressure ratios. Such results indicate that, for the wedge nozzle and related nozzle configurations, the two-dimensional, inviscid theory may be applied as a limited performance predictor.

INTRODUCTION

Multimission jet aircraft must operate effectively over a wide range of Mach numbers and power settings. Such aircraft require high-performance propulsion exhaust nozzles. Conventional axisymmetric nozzles are lightweight and use a variable geometry for high internal performance. As a result, the axisymmetric nozzle has generally been implemented in the multiengine jet aircraft design. However, the integration of multiple nozzles with the airframe results in a complex aft-end flow field, which can produce an aft-end drag problem. (See ref. 1.) In addition, the multiengine jet aircraft design generally requires a large boattail "gutter" interfairing between the engines or the nozzles. This interfairing increases the drag problem, especially in the case of separated flow near the nozzle exit (refs. 2 and 3).

The effects of such adverse interference may be minimized by the use of nonaxisymmetric wedge nozzle designs. Proper integration of a nonaxisymmetric design can eliminate the boattail "gutter" interfairing and, thus, reduce the adverse drag effects. (See ref. 4.) This nozzle also has the advantage of efficient in-flight thrust-reversing or

thrust-vectoring capabilities, unavailable in the conventional axisymmetric nozzle. (See ref. 5.) Preliminary research has indicated that the isolated aeropropulsive performance of the wedge nozzle compares favorably with that of axisymmetric nozzles at transonic and supersonic speeds. (See refs. 6 and 7.)

The available data base for nonaxisymmetric nozzle research is drawn from analysis of isolated and integrated nozzle designs (refs. 6 to 10). A small part of the data base includes pressure measurements and internal flow properties. (See ref. 11.) However, the data consist primarily of force measurements, which represent the nozzle aeropropulsive performance in terms of thrust and drag. The objective of this experiment is the addition of pressure measurements and internal flow field characteristics to the present data base. In this investigation, an isolated, nonaxisymmetric wedge nozzle has been tested extensively at static conditions. The resulting data consist of detailed pressure measurements for the internal flow field and the exhaust jet. Oil flow photographs provide additional flow field characteristics. Such data types are necessary for expanding the currently limited data base. An increased understanding of the flow phenomena is essential in the development of adequate prediction techniques.

In addition to this experimental investigation, an analysis has been performed to evaluate the use of a two-dimensional, time-dependent, inviscid theory as a nonaxisymmetric nozzle performance predictor. (See ref. 12.) A general, accurate prediction theory is essential for the development of high-performance nonaxisymmetric nozzles at minimum cost. Comparison of the experimental data and the analytical results evaluates the application of the theory as a predictor model under static conditions.

SYMBOLS

A_t	nozzle throat area, cm^2
b	width of trailing edge of nozzle wedge, cm
C_T	thrust coefficient, $T/A_t p_{t,j}$
ϵ	center line
c	crown (keel) line, cm (see fig. 3)
D	maximum nozzle diameter, cm
d	half-breadth line, cm (see fig. 3)

l	length of wedge from throat to trailing edge, cm
p	local static pressure, Pa
p_a	atmospheric pressure, Pa
$p_{t,j}$	jet total pressure, Pa
r	nozzle internal radius, cm
T	thrust, N
x	distance along model center line from nozzle throat, positive downstream, cm
y	vertical distance from plane passing through nozzle throat and center line, cm
z	lateral distance from plane passing through nozzle throat and center line, cm
η	order of superellipse equation
θ	angular component of (r, θ) polar coordinate system, rad (see fig. 3)

Abbreviations:

NAP	computer program for computation of two-dimensional, time-dependent, inviscid nozzle flow
SAE	Society of Automotive Engineers, Inc.

MODEL

The experiment was conducted using the base line, dry power configuration of the nonaxisymmetric wedge nozzle discussed in reference 6. Figure 1 contains a photograph of the model installed for static testing. The main features of this nozzle are the wedge-centerbody geometry and the nozzle internal area distribution.

Figure 2 gives the nozzle assembly dimensions and the wedge geometry. Duct-wedge cross sections of the internal flow area are given in the figure for the regions upstream of the leading edge of the wedge, at the leading edge, and at the geometric throat of the nozzle. The internal flow geometry is characterized by a transition from a circle

upstream of the wedge to a superellipse, a rectangular geometry, at the nozzle throat. The transition section is illustrated in figure 3. A detailed discussion of the transition and superellipse geometry is given in the appendix.

APPARATUS

The experimental investigation was conducted in the static test stand of the Langley 16-foot transonic tunnel. The air supply system is the same as that of the transonic tunnel. Reference 13 describes this facility in detail. The air control system is similar; it includes valving, filters, and heat exchange facilities. The data acquisition system, also similar to that of the 16-foot transonic tunnel, is based on a 100-channel magnetic tape system.

Figure 4 contains a photograph of the static test simulation system in the static test stand. An external high-pressure air system provided the air supply. Dry, heated air at a controlled stagnation temperature of 300 K entered a high-pressure chamber through six supply lines in the nozzle support. The flow of high-pressure air ran perpendicular to the model axis. From the high-pressure chamber, the flow entered the low-pressure plenum. Air passed from the low-pressure plenum to the nozzle tailpipe to simulate jet exhaust flow from the nozzle exit.

Instrumentation

This investigation included measurements of surface static pressure, jet total pressure, jet total temperature, and air mass-flow rate. The pressure values were recorded by seven multiple pressure scanning transducer units. A thermocouple was used to measure the jet total temperature in the low-pressure plenum. An electronic turbine flowmeter was used to record the mass flow of the high-pressure air. The pressure and temperature in each air supply line were also measured before the flow discharged into the low-pressure plenum.

The original model (ref. 6) was modified to include 286 pressure orifices, each 0.1016 cm in internal diameter. Rows of orifices were placed along the surface of the wedge, along the inner right sidewall of the cowl, and inside the top of the cowl. Each of these areas held three orifice rows. Most of the row positions can be seen in figure 1. Specific Cartesian coordinates of the pressure orifices, as well as diagrams of their location on the model, are given in table I.

On the nozzle wedge, all three orifice rows ran in the axial direction, with 0.635 cm between the successive orifices. One row was placed along the center line on the bottom of the wedge. The second row was placed along the left quarter span on top of the wedge.

The third row, also on top of the wedge, was located along the extreme right edge of the wedge sidewall.

Internal pressure orifices were placed along the top inside of the cowl. The rows ran in the axial direction, with 0.635-cm spacing between the orifices, as on the wedge. One row was placed along the axial center line; another ran along the left quarter span. The third row was placed along the inside of the upper left sidewall corner, with an inclination of approximately 45° from the center of the plane of the wedge.

Internal pressure orifices were placed horizontally along the right sidewall of the cowl up to the leading edge of the wedge. One row ran along the sidewall center line; the spacing between orifices in this row was 0.635 cm. The remaining two rows were placed 2.45 cm above the center line and 2.45 cm below the center line, respectively. Spacing in these rows was 1.27 cm between orifices.

Tests

Two types of experimental data were obtained: pressure distributions and oil flow photographs. The nozzle pressure distributions were determined for a range of nozzle pressure ratios from 1.5 to 6.0, at 0.5 increments. For the oil flow data, the orifices on the wedge were sealed, and the top of the wedge was painted black. For each nozzle pressure ratio, the wedge was covered with a thin coat of SAE 140 oil, and a high-speed photograph of the oil flow pattern was taken. As a secondary oil flow data system, a video tape of the developing and final flow field was made at each nozzle pressure ratio.

Experimental Data and Discussion

The pressure distributions and the oil flow photographs for the complete range of experimental data are given in figure 5. Pressure data are plotted as the ratio of local pressure to jet total pressure against the nozzle length, nondimensionalized by the distance from the throat to the end of the wedge. The oil flow photographs are scaled to the horizontal axis of the data plots.

The pressure distributions and oil flow photographs describe internal flow characteristics at each experimental nozzle pressure ratio. The results are discussed for each of the three data acquisition regions on the nozzle: along the internal cowl top, along the internal right sidewall, and along the wedge.

Cowl top.— Along the top of the cowl, the internal pressure distribution is essentially the same for the range of nozzle pressure ratios investigated. The flow chokes even at the lowest nozzle pressure ratio of 1.5. The critical pressure ratio of 0.528 occurs slightly downstream of the geometric throat, but ahead of the nozzle exit. A lack of significant spanwise variation indicates that the flow is essentially two-dimensional in this region.

Cowl right side.- Along the right side of the cowl, the pressure distribution far upstream lies in the stagnation chamber of the nozzle. The downstream measurements in this region are in the vicinity of the leading edge of the wedge. On the center orifice row, the pressures increase slightly as the wedge is approached. This increase in pressure results from the reduction in velocity which occurs as the flow approaches the stagnation region of the wedge. Along the top and bottom rows, the pressures decrease slightly, reflecting an increase in the subsonic velocity as the flow moves into the converging area of the nozzle. These flow patterns remain similar for the full range of experimental nozzle pressure ratios.

Wedge.- Along the surface of the wedge, the pressure distributions upstream of the nozzle exit are similar for all 10 nozzle pressure ratios investigated. The ratio of local pressure to jet pressure begins near unity upstream and decreases to the critical pressure ratio of 0.528 at the throat. In the upstream region and in the throat area, the flow is quasi two-dimensional, as has been discussed earlier. However, downstream of the throat and nozzle exit, the flow becomes three-dimensional, particularly for nozzle pressure ratios greater than 2.0. Three-dimensional flow patterns are illustrated by the data plots and oil flow photographs for the higher nozzle pressure ratios in figure 5. The pressure distributions, oil flow photographs, and video tape data were analyzed to determine the basic three-dimensional flow characteristics. A diagram of the dominant flow characteristics apparent at a nozzle pressure ratio of 6.0 is given in figure 6. The single flow characteristic which is evident at nozzle pressure ratios above 2.0 is a strong shock wave just downstream of the nozzle exit. The flow field observations indicate that turbulence effects due to the shock result in counterrotating vortex flow on either side of the wedge center line, slightly downstream of the shock. At the higher nozzle pressure ratios, apparent flow disturbance downstream indicates that a weaker secondary shock may occur downstream, in the vicinity of the trailing edge of the wedge. The pressure distribution near the wedge sidewall is essentially the atmospheric pressure, indicating a possible layer separation in this region.

The shock waves and vortex flow define three-dimensional flow along the wedge, downstream of the nozzle exit. Three-dimensional effects are dominant along the wedge center line for the higher nozzle pressure ratios. Viscous effects tend to decrease the magnitude of the pressure gradient along the center line in the vicinity of shock waves. As a result, the pressure variation is minimal along the center line. However, away from the center line, the viscous effects become weaker and exert limited influence on the magnitude of the pressure gradients. As a result, larger changes in pressure occur away from the center line, as illustrated by the variation in the wedge data at the higher nozzle pressure ratios. (See fig. 5.)

In summary, the flow through the nonaxisymmetric wedge nozzle may be divided into two regions, one of essentially two-dimensional flow and one of three-dimensional flow. Flow through the nozzle cowl is quasi two-dimensional until it passes the throat. For all experimental nozzle pressure ratios, the flow choked at this point. Downstream of the cowl, the jet flow along the wedge becomes highly three-dimensional. The dominant characteristics of the flow in this region include a strong shock wave and counter-rotating vortex flow.

ANALYTICAL INVESTIGATION

A two-dimensional, inviscid, time-dependent theory was applied to the nonaxisymmetric wedge nozzle as a potential predictor of the nozzle performance. This theory has been incorporated in the development of a computer program (NAP) which calculates internal nozzle flow and jet exhaust plume for steady converging, converging-diverging, and plug nozzle configurations (ref. 12). The external flow velocity is zero. Internal flow may be specified as either axisymmetric or two-dimensional.

The computer code incorporates the two-dimensional equations of motion in nonconservative form. A geometric computational grid spans the entire flow area. The interior mesh points are calculated by a MacCormack finite-difference scheme, a two-step predictor-corrector. The boundary mesh points, inlet and exit, are computed by a second-order reference plane method of characteristics. Shock waves are modeled using a "shock smearing" technique which incorporates an explicit artificial viscosity term with numerical smoothing. For this analysis the program output was generated as velocity, temperature, density, and pressure for grid points spanning the internal and external jet flow areas. The exhaust jet plume boundary and thrust values were also calculated.

To evaluate the two-dimensional theory as a nonaxisymmetric nozzle performance predictor, the computer-generated results were compared with the experimental data discussed previously. The internal flow characteristics and the jet plume boundary and flow characteristics were calculated using the wedge configuration under two-dimensional conditions. Since the experiment was conducted at static conditions, no external flow specification was necessary. Results are presented for seven cases; these cases range from nozzle pressure ratios of 3.0 to 6.0, at 0.5 increments. Analytical flow was not calculated below the nozzle pressure ratio of 3.0, since limitations in the computer code inhibit the flow velocity from returning to subsonic levels once it has become supersonic.

Several input parameters are important in achieving a stable solution with an acceptable level of accuracy. A convergence parameter controls the total number of iterations and the stability of the solution. The theory is also sensitive to an input initial estimate of the exhaust jet boundary in those cases which require a jet calculation. An inaccurate jet

plume boundary estimate may cause errors in the initial data surface and may result in a truncation of the solution process in its early iterative stages.

The convergence of a solution is based on the amount of change in maximum velocity between two consecutive time steps. The maximum horizontal velocity over the full computational region is found at each time step. The percentage difference between the maximum velocity at a current time step and the value of maximum velocity at the preceding time step is then computed. When the percentage change in velocity falls below the input-specified convergence parameter, the solution reaches convergence, and the iterative process stops. Thus, the convergence parameter reflects the stability of the calculated flow velocity. The convergence parameter, the final number of iterations, and the time step size for each case are given in table II.

Comparison of Theory and Experiment

Figure 7 compares the NAP analytical results with the experimental data for seven nozzle pressure ratios. The analytical results were calculated along the axial center line of the wedge and the top inside center line of the cowl. The computer program output is compared with the experimental data along the center line and along the quarter span for both the wedge and the inside top of the cowl.

On the cowl top, there is good agreement between the two-dimensional theory and the experiment for the full range of nozzle pressure ratios. The NAP center-line results agree well with the experimental data along both the quarter span and the center line. The experimental data indicate that the flow along the top of the cowl is essentially two-dimensional, with no spanwise variation. Viscous effects are negligible in this region. Because of the two-dimensional, inviscid nature of the flow, the experimental quarter-span data and center-line data are so similar that the NAP predictions agree with both data sets. Thus, the two-dimensional inviscid theory is an accurate flow model for the internal flow along the top region of the cowl.

Along the wedge, the theory and experiment agree well in the internal flow regions for all seven cases. In the exhaust jet, the comparison between analytical and experimental results shows rather limited agreement. For the experimental center-line data, the agreement with the computed results is only fair for the nozzle pressure ratios above 4.5, but improves as the nozzle pressure ratio drops to 3.0. The general lack of agreement at the higher pressure ratios results from the complex, three-dimensional nature of the exhaust jet flow field, as discussed previously. For these cases, a two-dimensional, inviscid theory is inadequate for predicting such highly three-dimensional flow characteristics. As the nozzle pressure ratio drops, however, so does the magnitude of the flow disturbances along the center line, and the theory-experiment comparison improves in the center-line region.

The analytical results and the quarter-span experimental data for the jet region show better agreement than the center-line comparisons, except at the higher nozzle pressure ratios. For the higher pressure ratios, the strong three-dimensional effects dominate the entire jet region. At the lower nozzle pressure ratios, the viscous effects tend to damp out the strong shock effects, so that the three-dimensional flow characteristics along the quarter span diminish in magnitude. Since the flow is more two dimensional in these cases, the results of the two-dimensional, inviscid theory compare favorably with the quarter-span data.

In addition to the pressure distributions, analytical gross thrust values were calculated for all seven nozzle pressure ratios. These predictions were compared with experimental data for the wedge nozzle, which are presented in reference 6. The experimental and analytical results are given in figure 8 as thrust coefficients at each nozzle pressure ratio. The coefficients of the ideal isentropic gross thrust, as calculated in reference 6, are also plotted. The predicted thrust coefficients generally lie between the ideal and experimental values. However, agreement is rather inconsistent, reflecting the lack of agreement in certain experimental and analytical pressure distributions, as discussed previously. Thus, for the wedge nozzle, the theoretical thrust prediction is rather limited. Results for other types of nozzles indicate an improvement in prediction of thrust or discharge coefficient, as is discussed briefly in reference 12.

The two-dimensional, inviscid, time-dependent theory is a good performance predictor for the wedge nozzle in the internal regions where flow is essentially two-dimensional. In regions of three-dimensional flow, the theory gives reasonable approximations to the flow field characteristics at lower nozzle pressure ratios, where the viscous effects are minimized. At higher nozzle pressure ratios, the theory is inadequate for prediction of highly three-dimensional flow. Thus, for the wedge nozzle and similar configurations, the two-dimensional, inviscid theory may be applied as a limited performance predictor of internal and jet flow characteristics.

CONCLUSION

An experimental investigation of a nonaxisymmetric wedge nozzle has been conducted at static conditions. The resulting detailed pressure distributions and oil flow photographs expand the current nonaxisymmetric data base, which consists primarily of thrust and drag data. In addition, an analytical investigation has been made to evaluate a two-dimensional, inviscid, time-dependent theory as a nonaxisymmetric nozzle performance predictor. In the regions of two-dimensional nozzle flow, the analytical results agree well with the experimental data for the full range of nozzle pressure ratios under investigation.

In regions of three-dimensional flow, the theory predicts the basic flow characteristics of the real data; the agreement of theory with experiment is optimum at the lower nozzle pressure ratios, where three-dimensional effects are minimum. Results indicate that for the wedge nozzle and similar designs, the two-dimensional, inviscid, time-dependent theory may be applied as a limited performance predictor of internal and jet flow characteristics.

Langley Research Center
National Aeronautics and Space Administration
Hampton, VA 23665
May 2, 1958

APPENDIX

TRANSITION GEOMETRY

The internal geometry of the nonaxisymmetric wedge nozzle is characterized by a region of transition from a circular flow area to a rectangular area. This transition section is illustrated in figure 3. The section begins upstream of the leading edge of the wedge and ends at the nozzle geometric throat. The subsequent equations define the superellipse, or rectangular, geometry and the area distribution of the flow region. The cross sections are defined by r , θ , c , d , and η in the form

$$r^\eta = \left[\frac{1}{\left(\frac{\sin \theta}{c}\right)^\eta + \left(\frac{\cos \theta}{d}\right)^\eta} \right]$$

The coordinates y and z may then be computed at each x , using

$$y = r \sin \theta$$

$$z = r \cos \theta$$

The duct internal geometry is based on the parameters c , d , and η , used in the superellipse equation. The dimensions shown in the subsequent equations define the internal duct geometry of the static test model. All dimensions are in centimeters.

For $-17.600 \leq x \leq -13.830$

$$c = 6.286$$

$$d = 6.286$$

$$\eta = 2.0$$

For $-13.830 \leq x \leq -6.915$

$$x_1 = \frac{x + 13.830}{6.915}$$

$$x_2 = \frac{\sin \left[\pi (x_1 + 1.5) \right] + 1}{2}$$

APPENDIX

$$d = 6.287 - (0.095)x_2$$

$$x_3 = \frac{x + 13.830}{13.830}$$

$$x_4 = \frac{\sin\left[\pi\left(x_3 + 1.5\right)\right] + 1.0}{2.0}$$

$$x_5 = 1.0 + \left(2048\sqrt{2} - 1.0\right)x_4$$

$$\eta = \frac{\ln 2}{\ln \frac{\sqrt{2}}{x_5}}$$

The cross-sectional area is fixed in this region. To find c , iterate

$$\left(\frac{y}{c}\right)^\eta + \left(\frac{z}{d}\right)^\eta = 1$$

At $x = -6.915$

$$c = 6.250$$

$$d = 6.191$$

$$\eta = 3.559$$

For $-6.915 \leq x \leq 0$

$$d = 6.191$$

$$x_1 = \frac{x + 6.915}{6.915}$$

$$x_2 = \frac{\sin\left[\pi\left(x_1 + 1.5\right)\right] + 1}{2}$$

APPENDIX

$$x_3 = 0.75 - 0.5x_2$$

$$c_1 = c \quad \text{at } (x = -6.915) = 6.2504$$

$$c = c_1 + (6.2865 - c_1) (x_2)^{x_3}$$

$$x_4 = \frac{x + 13.830}{13.830}$$

$$x_5 = \frac{\sin[\pi(x_4 + 1.5)] + 1.0}{2.0}$$

$$x_6 = 1 + (2048\sqrt{2} - 1.0)x_5$$

$$\eta = \frac{\ln 2}{\ln \frac{\sqrt{2}}{x_6}}$$

For $0 \leq x \leq 26.505$

$$c = 6.2865$$

$$d = 6.1913$$

$$\eta = 11.0$$

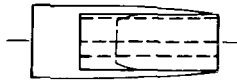
REFERENCES

1. Schmeer, James W.; Lauer, Rodney F., Jr.; and Berrier, Bobby L.: Performance of Blow-in-Door Ejector Nozzles Installed on a Twin-Jet Variable-Wing-Sweep Fighter Airplane Model. NASA TM X-1383, 1967.
2. Reubush, David E.; and Mercer, Charles E.: Effects of Nozzle Interfiring Modifications on Longitudinal Aerodynamic Characteristics of a Twin-Jet, Variable-Wing-Sweep Fighter Model. NASA TN D-7817, 1975.
3. Maiden, Donald L.; and Berrier, Bobby L.: Effect of Airframe Modifications on Longitudinal Aerodynamic Characteristics of a Fixed-Wing, Twin-Jet Fighter Airplane Model. NASA TM X-2523, 1972.
4. Maiden, Donald L.; and Petit, John E.: Investigation of Two-Dimensional Wedge Exhaust Nozzles for Advanced Aircraft. *J. Aircraft*, vol. 13, no. 10, Oct. 1976, pp. 809-816.
5. Capone, Francis J.: Supercirculation Effects Induced by Vectoring a Partial-Span Rectangular Jet. *J. Aircraft*, vol. 12, no. 8, Aug. 1975, pp. 633-638.
6. Maiden, Donald L.: Performance of an Isolated Two-Dimensional Variable-Geometry Wedge Nozzle With Translating Shroud and Collapsing Wedge at Speeds Up to Mach 2.01. NASA TN D-7906, 1975.
7. Maiden, Donald L.: Performance of an Isolated Two-Dimensional Wedge Nozzle With Fixed Cowl and Variable Wedge Centerbody at Mach Numbers Up to 2.01. NASA TN D-8218, 1976.
8. Martens, Richard E.: F-15 Nozzle/Afterbody Integration. *J. Aircraft*, vol. 13, no. 5, May 1976, pp. 327-333.
9. Capone, Francis J.; and Maiden, Donald L.: Performance of Twin Two-Dimensional Wedge Nozzles Including Thrust Vectoring and Reversing Effects at Speeds Up to Mach 2.20. NASA TN D-8449, 1977.
10. Pendergraft, O. C.: Comparison of Axisymmetric and Nonaxisymmetric Nozzles Installed on the F-15 Configuration. AIAA Paper 77-842, July 1977.
11. Harrington, Douglas E.; Schloemer, James J.; and Skebe, Stanley A.: Thrust Performance of Isolated Two-Dimensional Suppressed Plug Nozzles With and Without Ejectors at Mach Numbers From 0 to 0.45. NASA TM X-3384, 1976.

12. Cline, M. C.: NAP: A Computer Program for the Computation of Two-Dimensional, Time-Dependent, Inviscid Nozzle Flow. LA-5984 (Contract W-7405-ENG-36), Los Alamos Scientific Lab., Jan. 1977.
13. Corson, Blake W., Jr.; Runckel, Jack F.; and Igoe, William B.: Calibration of the Langley 16-Foot Transonic Tunnel With Test Section Air Removal. NASA TR R-423, 1974.

TABLE I.- PRESSURE ORIFICE LOCATIONS

[Coordinate system is defined in fig. 2]



Pressure orifice rows are indicated by dashed lines.

Wedge

(a) Center line

x/l	y/l	z/l	x/l	y/l	z/l
-0.263	-0.023	0	0.356	-0.112	0
-.250	-.044	0	.380	-.107	0
-.234	-.062	0	.403	-.103	0
-.218	-.078	0	.427	-.099	0
-.199	-.092	0	.451	-.095	0
-.179	-.107	0	.475	-.091	0
-.160	-.118	0	.498	-.087	0
-.139	-.130	0	.522	-.083	0
-.116	-.141	0	.545	-.078	0
-.093	-.150	0	.569	-.074	0
-.071	-.158	0	.593	-.070	0
-.048	-.164	0	.617	-.066	0
-.024	-.169	0	.640	-.062	0
0	-.170	0	.664	-.058	0
.024	-.169	0	.688	-.053	0
.048	-.165	0	.712	-.049	0
.072	-.161	0	.736	-.045	0
.098	-.157	0	.759	-.041	0
.121	-.153	0	.783	-.037	0
.144	-.149	0	.806	-.033	0
.168	-.145	0	.830	-.029	0
.192	-.140	0	.854	-.024	0
.215	-.136	0	.878	-.020	0
.240	-.132	0	.901	-.016	0
.262	-.128	0	.927	-.012	0
.285	-.124	0	.949	-.008	0
.309	-.120	0	.973	-.004	0
.333	-.116	0			

(b) Left quarter span

x/l	y/l	z/l	x/l	y/l	z/l
-0.263	0.024	-0.119	0.352	0.113	-0.119
-.252	.042	-.119	.376	.109	-.119
-.235	.061	-.119	.399	.105	-.119
-.219	.077	-.120	.423	.101	-.119
-.201	.092	-.119	.447	.097	-.120
-.180	.106	-.120	.470	.093	-.119
-.160	.119	-.119	.494	.089	-.119
-.140	.130	-.120	.518	.085	-.119
-.117	.140	-.120	.541	.081	-.119
-.096	.149	-.120	.565	.077	-.119
-.074	.157	-.119	.589	.072	-.119
-.051	.163	-.120	.613	.068	-.119
-.028	.168	-.120	.636	.064	-.120
-.005	.170	-.120	.660	.060	-.120
.020	.169	-.120	.684	.056	-.120
.044	.166	-.120	.707	.052	-.119
.068	.162	-.119	.731	.050	-.119
.092	.158	-.119	.755	.044	-.119
.116	.154	-.119	.778	.040	-.119
.139	.150	-.119	.802	.036	-.119
.164	.146	-.119	.826	.032	-.119
.187	.141	-.119	.849	.028	-.119
.210	.138	-.119	.874	.023	-.120
.234	.133	-.119	.898	.019	-.120
.258	.129	-.119	.922	.015	-.120
.283	.125	-.119	.945	.011	-.120
.305	.121	-.119	.969	.008	-.120
.328	.117	-.119			

(c) Right edge

x/l	y/l	z/l	x/l	y/l	z/l
-0.263	0.024	0.230	0.352	0.114	0.229
-.251	.044	.230	.376	.110	.229
-.236	.062	.230	.400	.106	.229
-.220	.077	.230	.423	.102	.229
-.199	.094	.230	.447	.098	.229
-.181	.106	.230	.470	.094	.230
-.159	.120	.230	.494	.090	.229
-.139	.130	.230	.518	.086	.229
-.117	.141	.229	.541	.082	.229
-.095	.150	.229	.565	.077	.229
-.074	.158	.229	.589	.073	.229
-.052	.164	.229	.612	.069	.229
-.028	.169	.229	.636	.065	.229
-.005	.171	.229	.660	.061	.229
.019	.170	.229	.683	.057	.229
.044	.167	.229	.707	.053	.229
.068	.163	.229	.731	.049	.230
.092	.159	.230	.756	.045	.229
.115	.155	.230	.778	.041	.228
.139	.151	.230	.802	.036	.228
.163	.147	.230	.826	.032	.228
.186	.143	.230	.850	.028	.228
.210	.138	.229	.874	.024	.228
.234	.134	.229	.897	.020	.228
.257	.130	.229	.921	.016	.228
.282	.126	.229	.944	.012	.228
.305	.122	.230	.968	.009	.228
.328	.118	.230			

TABLE I.- Concluded



Pressure orifice rows are indicated
by dashed lines.

Cowl top

(a) Center line

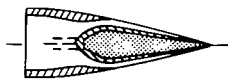
x/l	y/l	z/l	x/l	y/l	z/l
-0.619	0.239	0	-0.282	0.211	0
-.594	.239	0	-.258	.211	0
-.570	.239	0	-.234	.214	0
-.547	.239	0	-.210	.218	0
-.522	.238	0	-.186	.223	0
-.499	.237	0	-.161	.227	0
-.474	.235	0	-.138	.232	0
-.450	.231	0	-.114	.236	0
-.425	.228	0	-.090	.238	0
-.401	.224	0	-.066	.239	0
-.377	.220	0	-.042	.239	0
-.353	.217	0	-.018	.239	0
-.328	.214	0	.006	.240	0
-.306	.212	0			

(b) Left quarter span

x/l	y/l	z/l	x/l	y/l	z/l
-0.619	0.209	-0.116	-0.281	0.204	-0.118
-.595	.208	-.116	-.258	.206	-.118
-.571	.208	-.116	-.232	.211	-.118
-.546	.208	-.116	-.210	.216	-.118
-.522	.208	-.116	-.186	.221	-.118
-.499	.208	-.116	-.162	.226	-.118
-.475	.208	-.116	-.137	.231	-.118
-.450	.207	-.117	-.114	.235	-.117
-.425	.206	-.117	-.090	.238	-.117
-.402	.206	-.117	-.066	.239	-.117
-.378	.206	-.117	-.042	.239	-.117
-.354	.205	-.117	-.018	.239	-.117
-.329	.204	-.117	.006	.241	-.117
-.303	.202	-.117			

(c) Left corner

x/l	y/l	z/l	x/l	y/l	z/l
-0.619	0.155	-0.182	-0.282	0.171	-0.195
-.594	.157	-.180	-.256	.177	-.197
-.573	.154	-.183	-.233	.182	-.202
-.551	.152	-.184	-.209	.187	-.207
-.527	.152	-.185	-.185	.193	-.212
-.502	.154	-.185	-.161	.198	-.217
-.476	.155	-.185	-.137	.202	-.221
-.452	.156	-.186	-.113	.207	-.225
-.428	.156	-.189	-.089	.209	-.228
-.408	.160	-.188	-.065	.211	-.230
-.381	.162	-.189	-.041	.213	-.230
-.355	.162	-.192	-.016	.213	-.230
-.332	.167	-.191	.008	.213	-.230
-.302	.169	-.194			



Pressure orifice rows are indicated
by dashed lines.

Cowl right side

(a) Center line

x/l	y/l	z/l	x/l	y/l	z/l
-0.614	0	0.237	-0.445	0	0.237
-.587	0	.237	-.420	0	.237
-.564	0	.237	-.396	0	.236
-.539	0	.238	-.370	0	.236
-.516	0	.238	-.346	0	.236
-.492	0	.238	-.321	0	.236
-.467	0	.237	-.299	0	.236
			-.275	0	.235

(b) Below center line

x/l	y/l	z/l
-0.469	-0.095	0.220
-.419	-.095	.223
-.372	-.095	.226
-.323	-.096	.228
-.275	-.095	.231

(c) Above center line

x/l	y/l	z/l
-0.468	0.096	0.220
-.420	.096	.223
-.370	.096	.226
-.324	.097	.228
-.270	.095	.231

TABLE II.- CONVERGENCE CRITERIA

$p_{t,j}/p_a$	Convergence parameter	Total iterations	Step size, sec
3	0.005	8175	0.76×10^{-6}
3.5	.005	5181	$.79 \times 10^{-6}$
4	.005	3915	$.79 \times 10^{-6}$
4.5	.005	3422	$.78 \times 10^{-6}$
5	.006	3441	$.78 \times 10^{-6}$
5.5	.005	4034	$.78 \times 10^{-6}$
6	.007	3671	$.78 \times 10^{-6}$

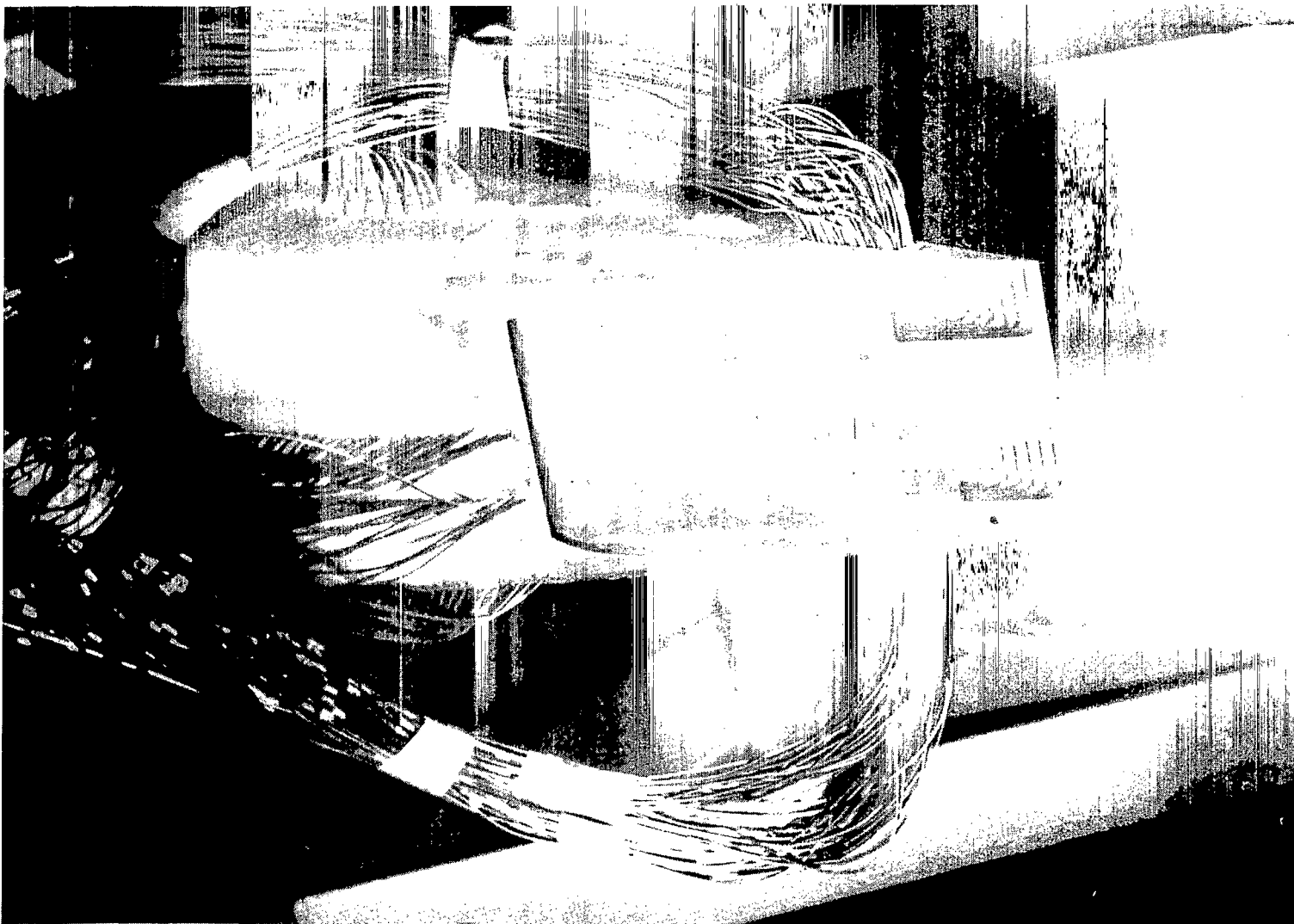
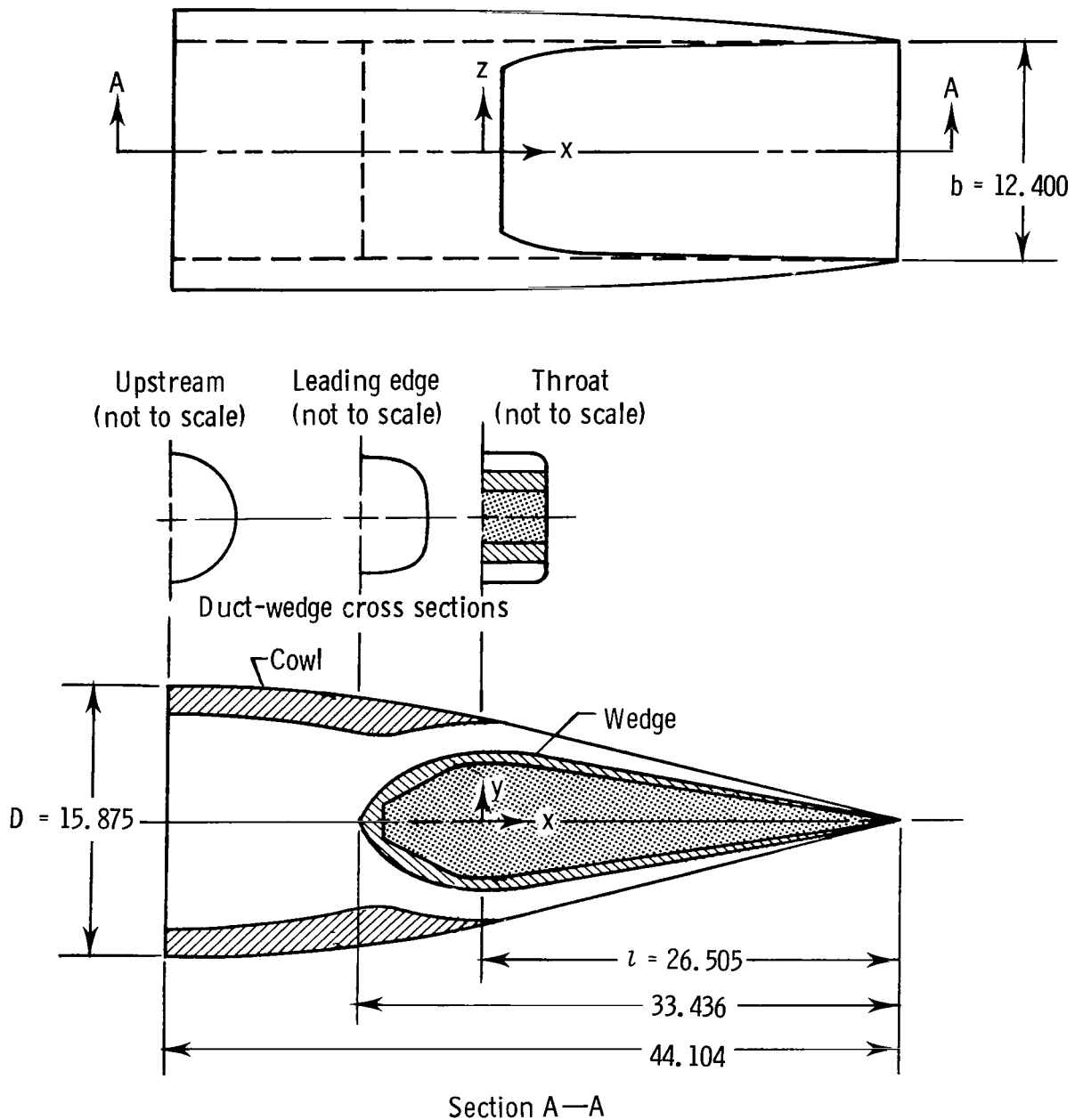


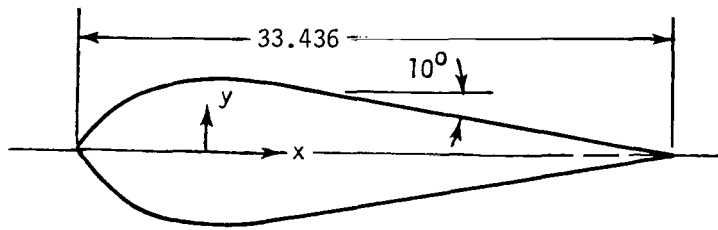
Figure 1.- Closeup view of nozzle installed for testing.

L-77-1524



(a) General design overview.

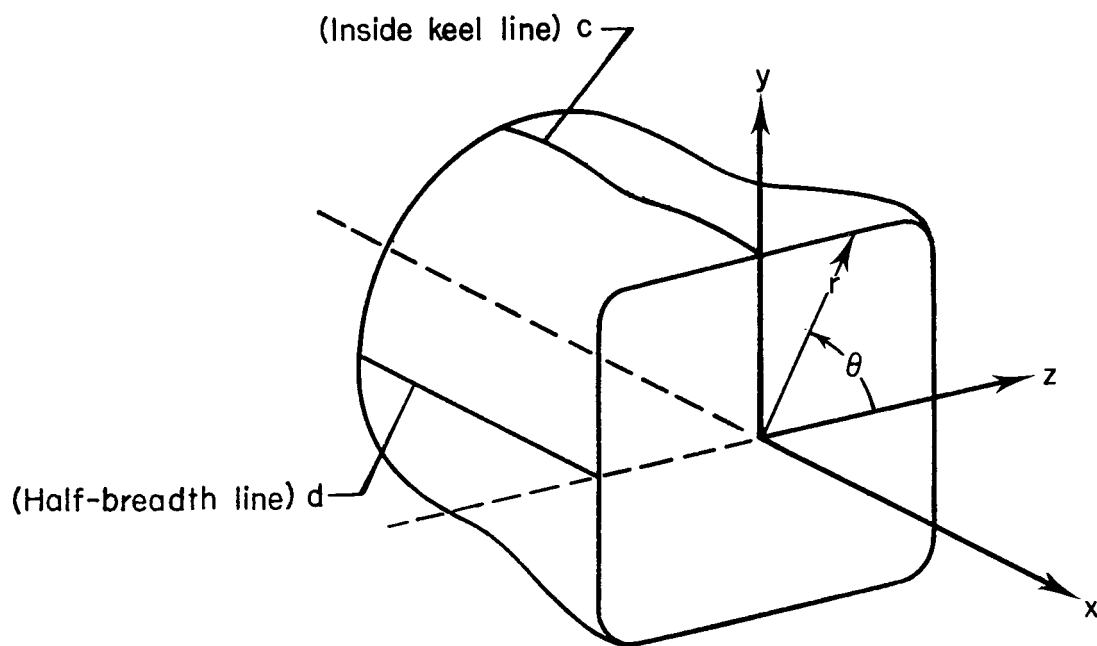
Figure 2.- Nozzle assembly dimensions. All dimensions are in cm.



Wedge coordinates	
x	y
-6.931	0.000
-6.238	1.321
-5.544	2.032
-4.851	2.540
-4.157	3.048
-3.464	3.353
-2.770	3.708
-2.077	3.962
-1.384	4.204
-.069	4.382
-.003	4.470
.069	4.394
1.390	4.428
26.505	.000

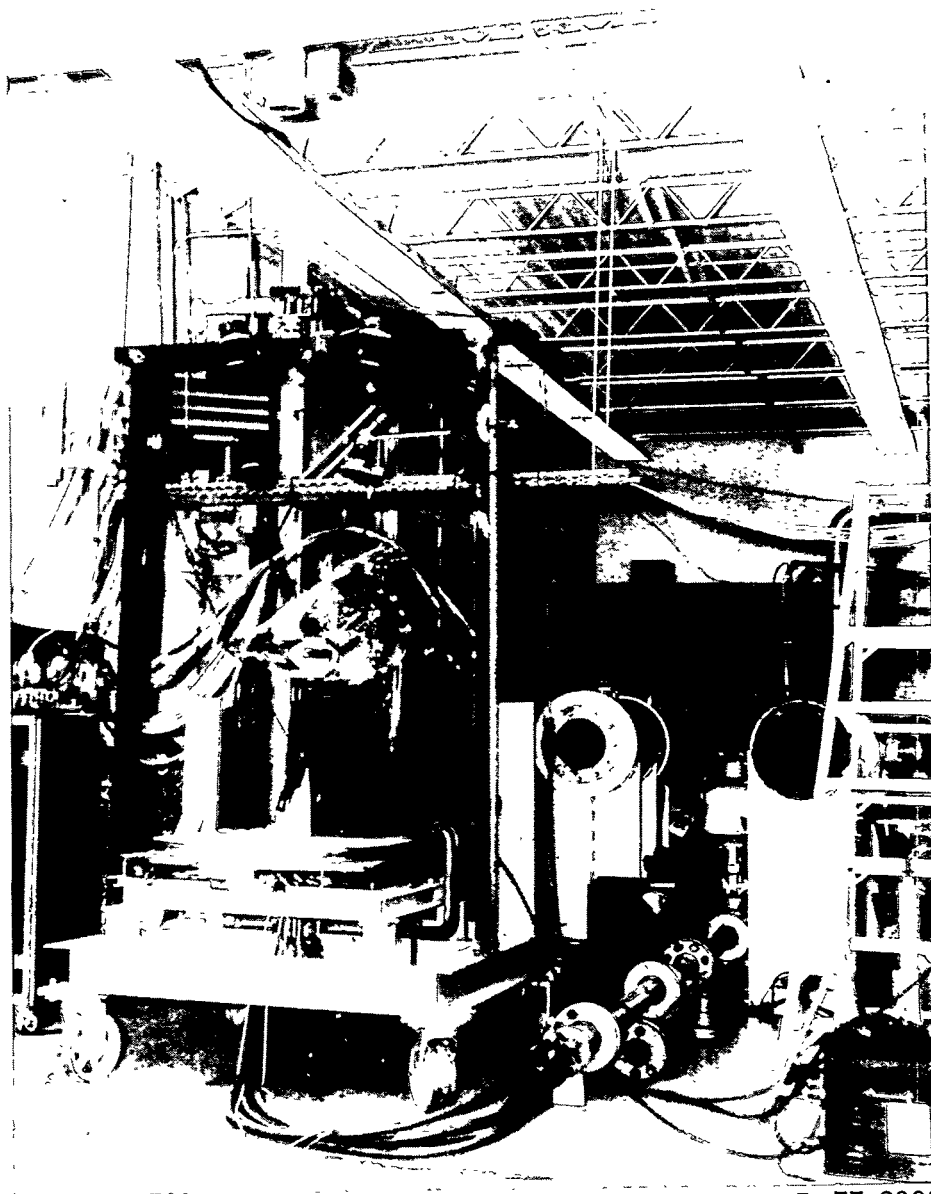
(b) Two-dimensional wedge geometry.

Figure 2.- Concluded.



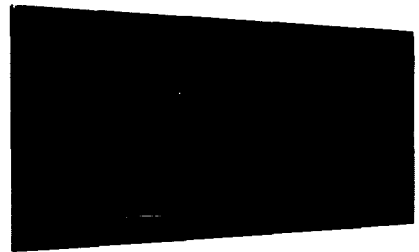
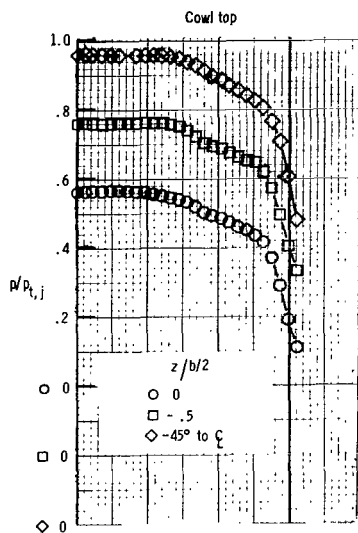
$$r^{\eta} = \left[\frac{1}{\left(\frac{\sin \theta}{c}\right)^{\eta} + \left(\frac{\cos \theta}{d}\right)^{\eta}} \right]$$

Figure 3.- Transition area internal geometry (coordinate system is defined in fig. 2).



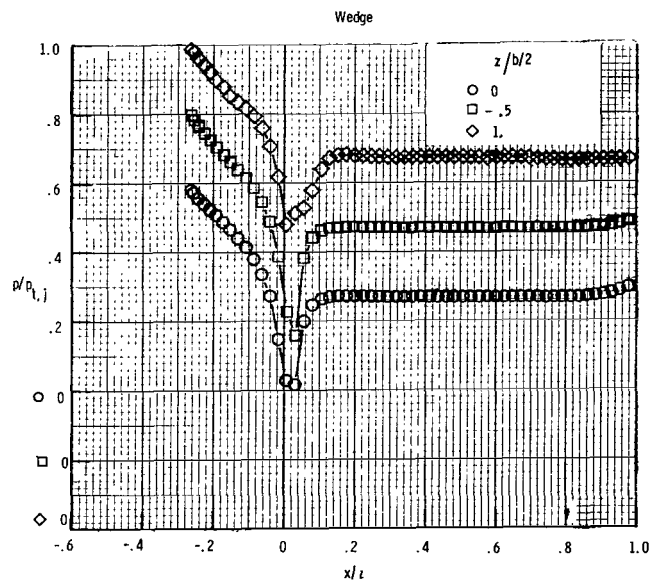
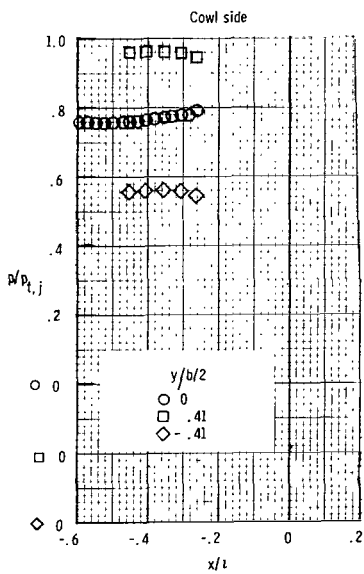
L-77-2098

Figure 4.- Overall view of test setup.



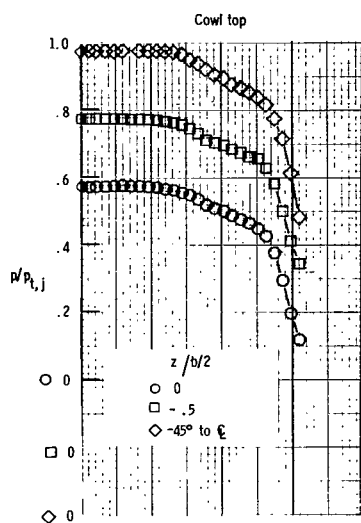
L-78-84

Wedge oil flow pattern



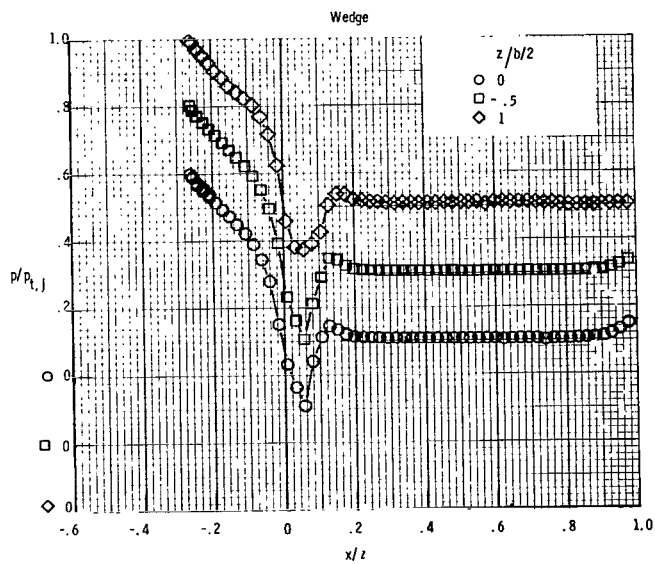
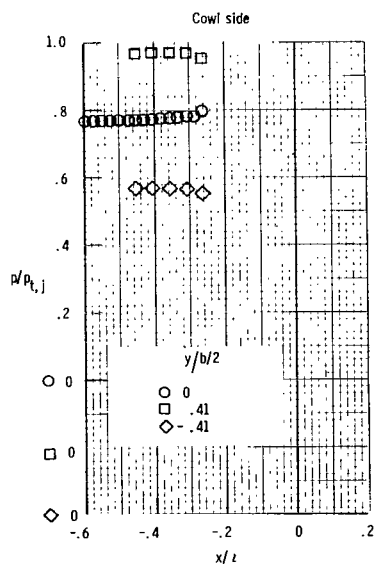
(a) $p_{t,j}/p_a = 1.5$.

Figure 5.- Nozzle pressure distribution and corresponding oil flow pattern.



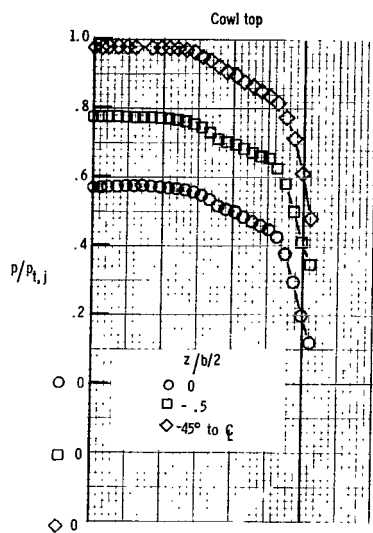
L-78-85

Wedge oil flow pattern



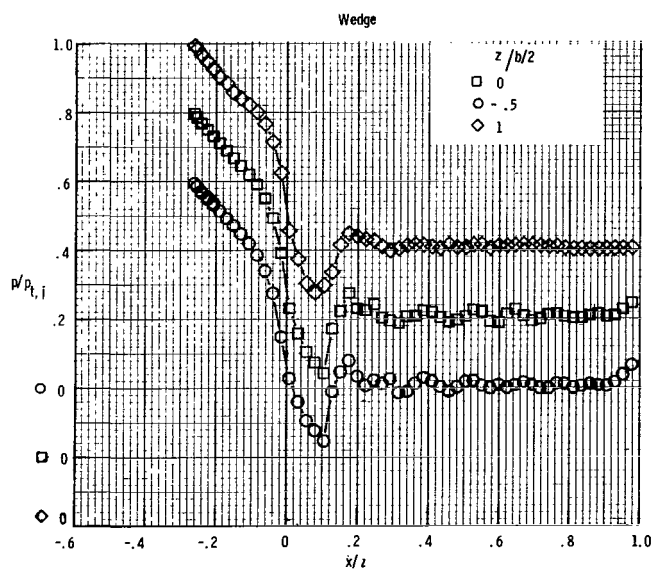
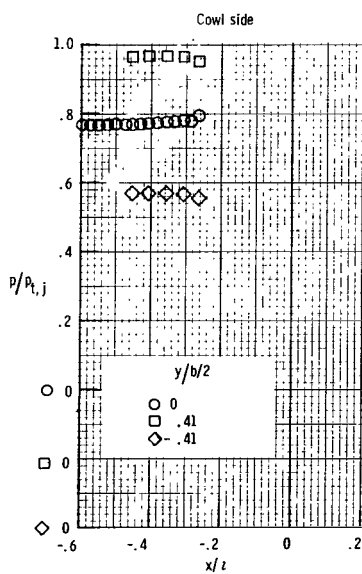
(b) $p_{t,j}/p_a = 2.0$.

Figure 5.- Continued.



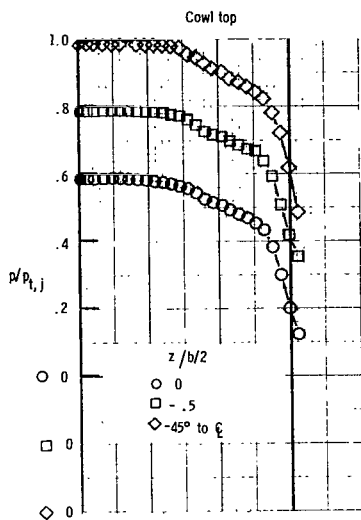
L-78-86

Wedge oil flow pattern



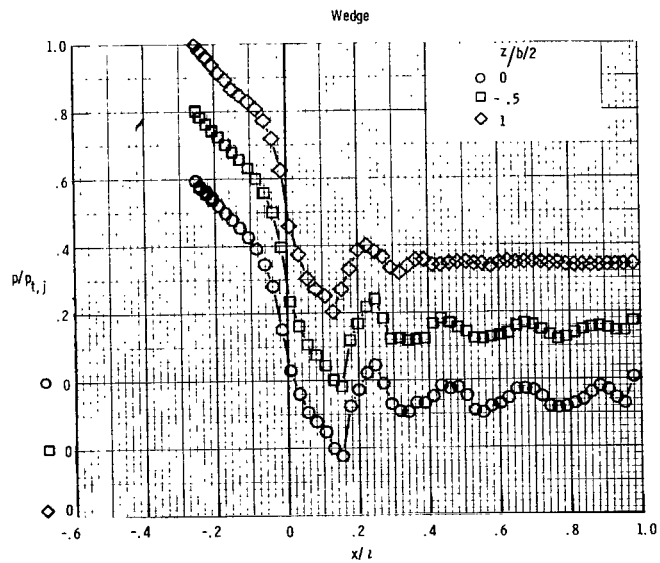
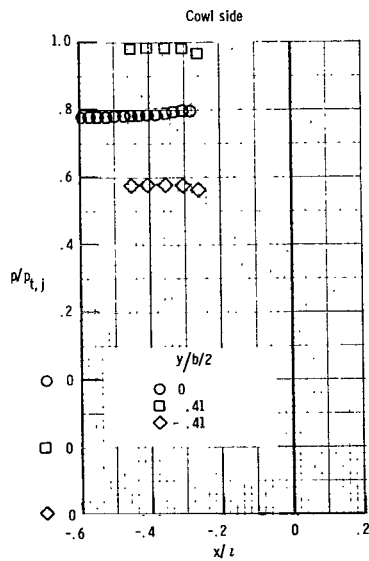
(c) $p_{t,j}/p_a = 2.5$.

Figure 5.- Continued.



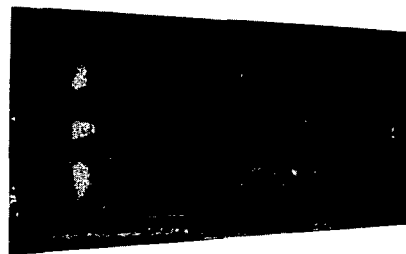
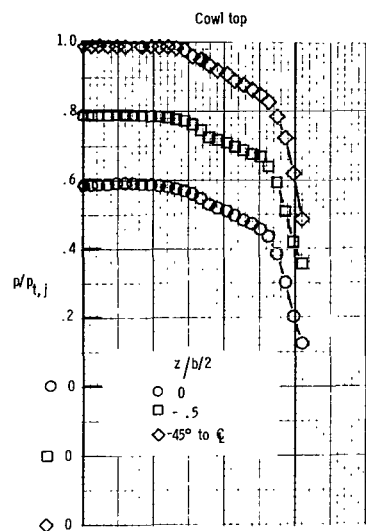
L-78-87

Wedge oil flow pattern



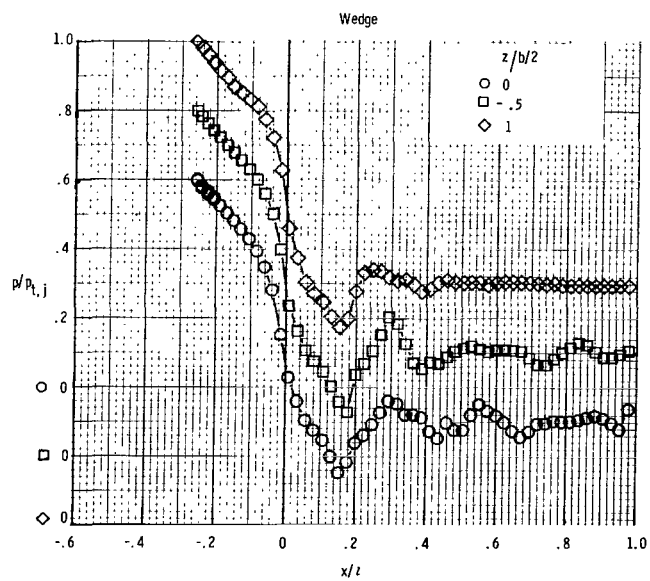
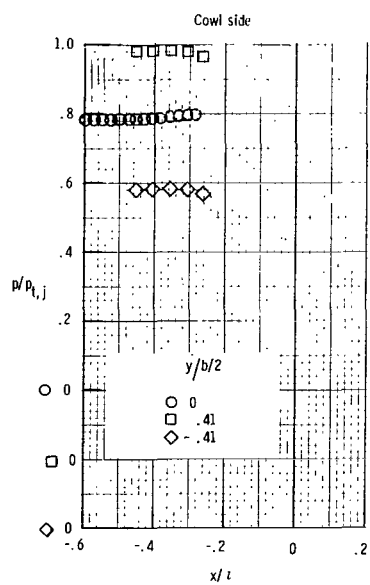
(d) $p_{t,j}/p_a = 3.0$.

Figure 5.- Continued.



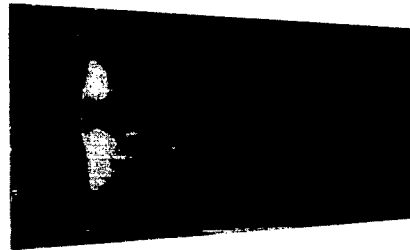
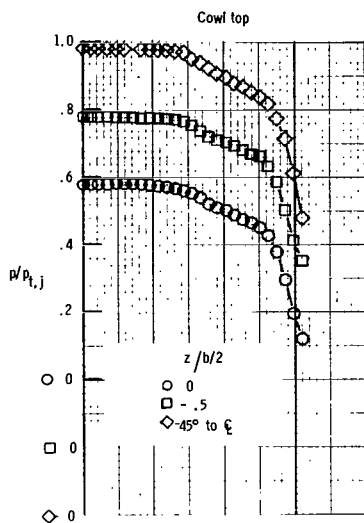
L-78-88

Wedge oil flow pattern



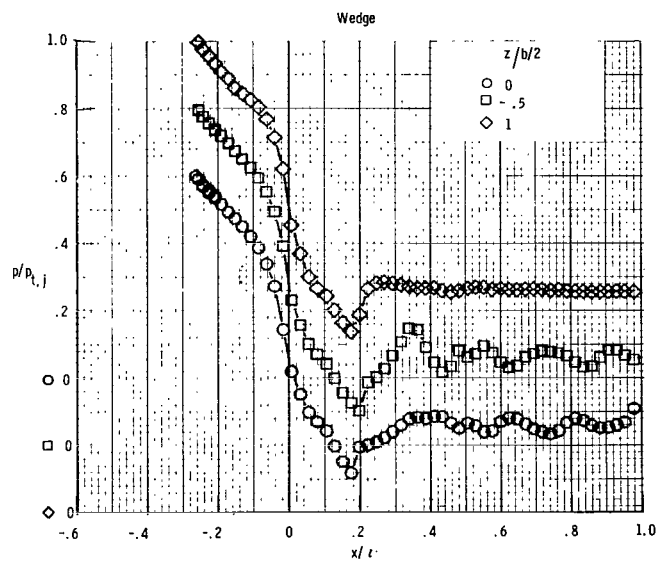
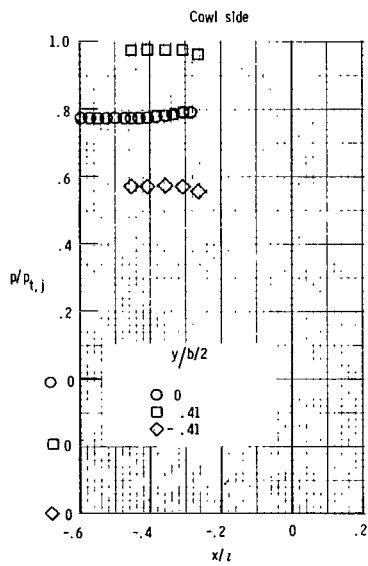
(e) $p_{t,j}/p_a = 3.5$.

Figure 5.- Continued.



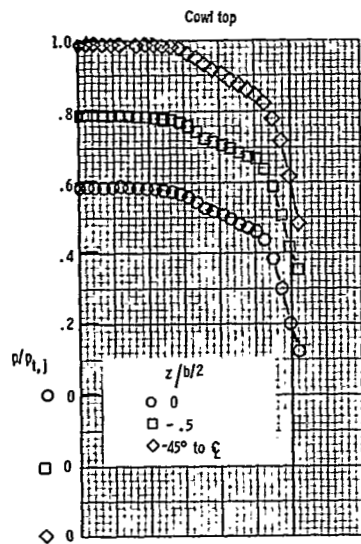
L-78-89

Wedge oil flow pattern



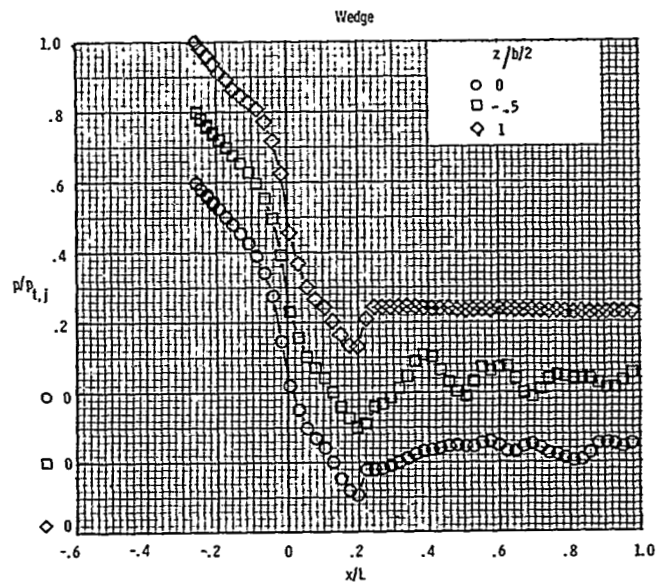
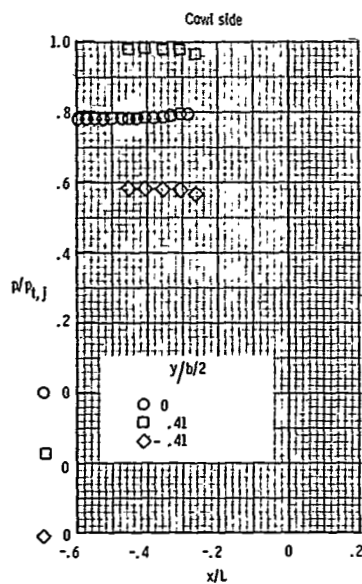
(f) $p_{t,j}/p_a = 4.0$.

Figure 5.- Continued.



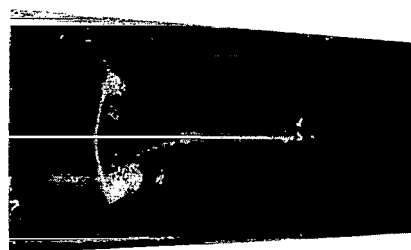
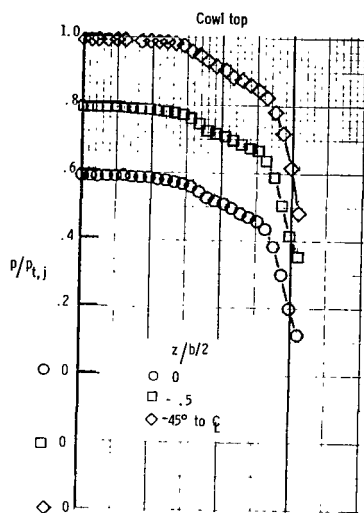
L-78-90

Wedge oil flow pattern



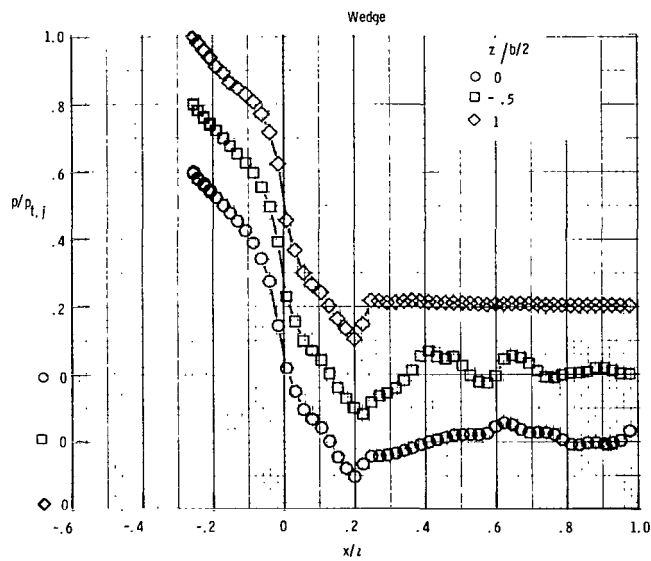
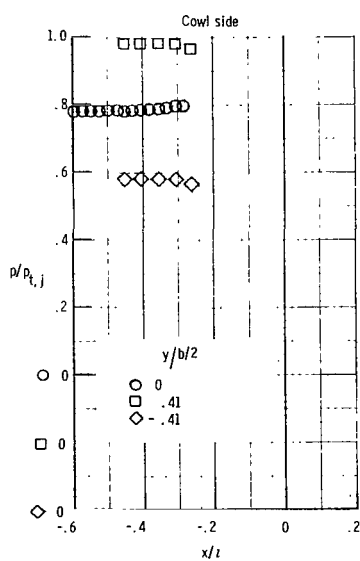
(g) $p_{t,j}/p_a = 4.5$.

Figure 5.- Continued.



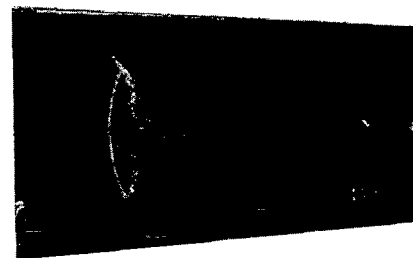
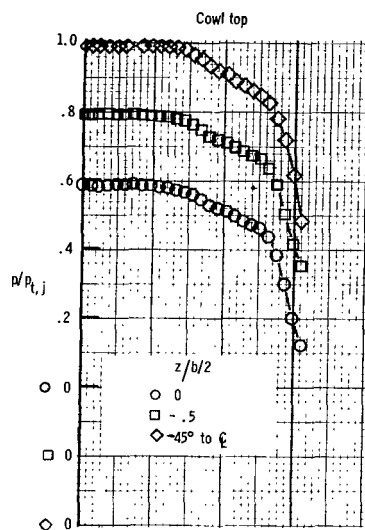
L-78-91

Wedge oil flow pattern



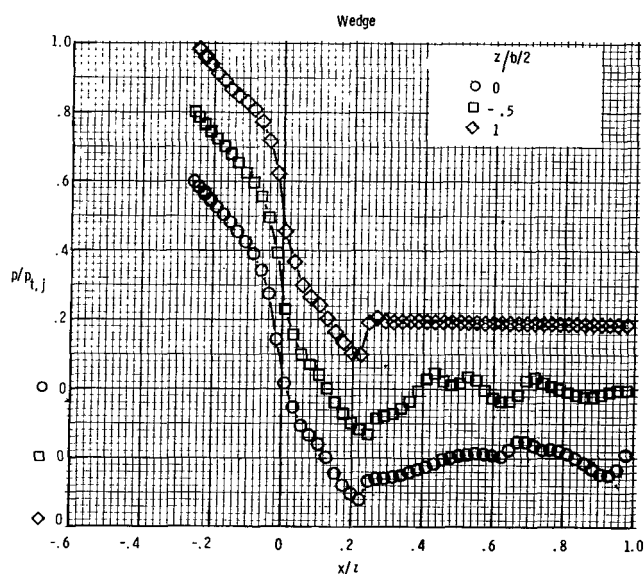
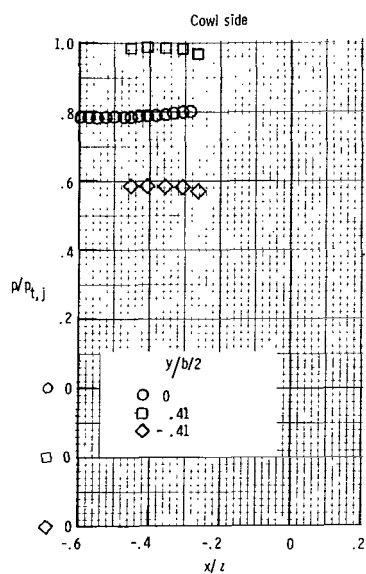
(h) $p_{t,j}/p_a = 5.0$.

Figure 5.- Continued.



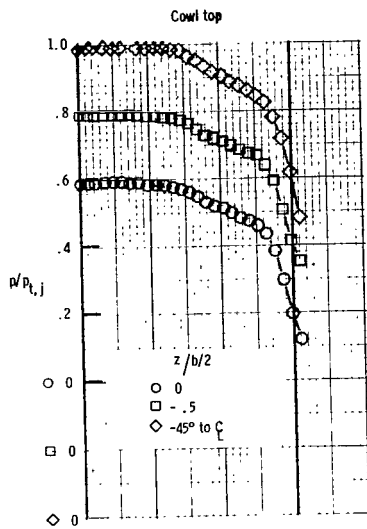
L-78-92

Wedge oil flow pattern



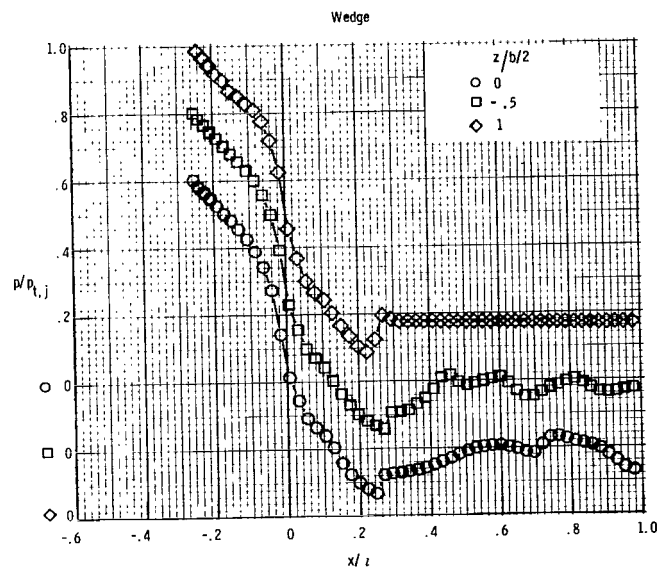
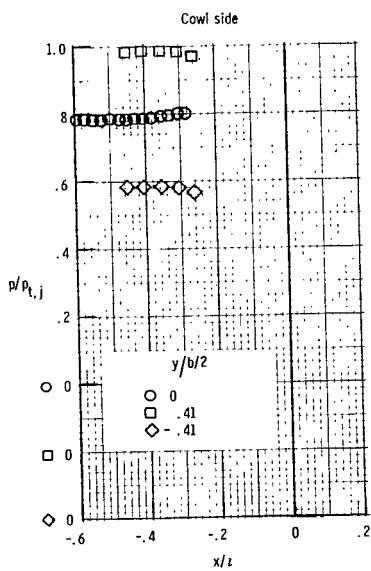
(i) $p_{t,j}/p_a = 5.5$.

Figure 5.- Continued.



L-78-93

Wedge oil flow pattern



(j) $p_{t,j}/p_a = 6.0$.

Figure 5.- Concluded.

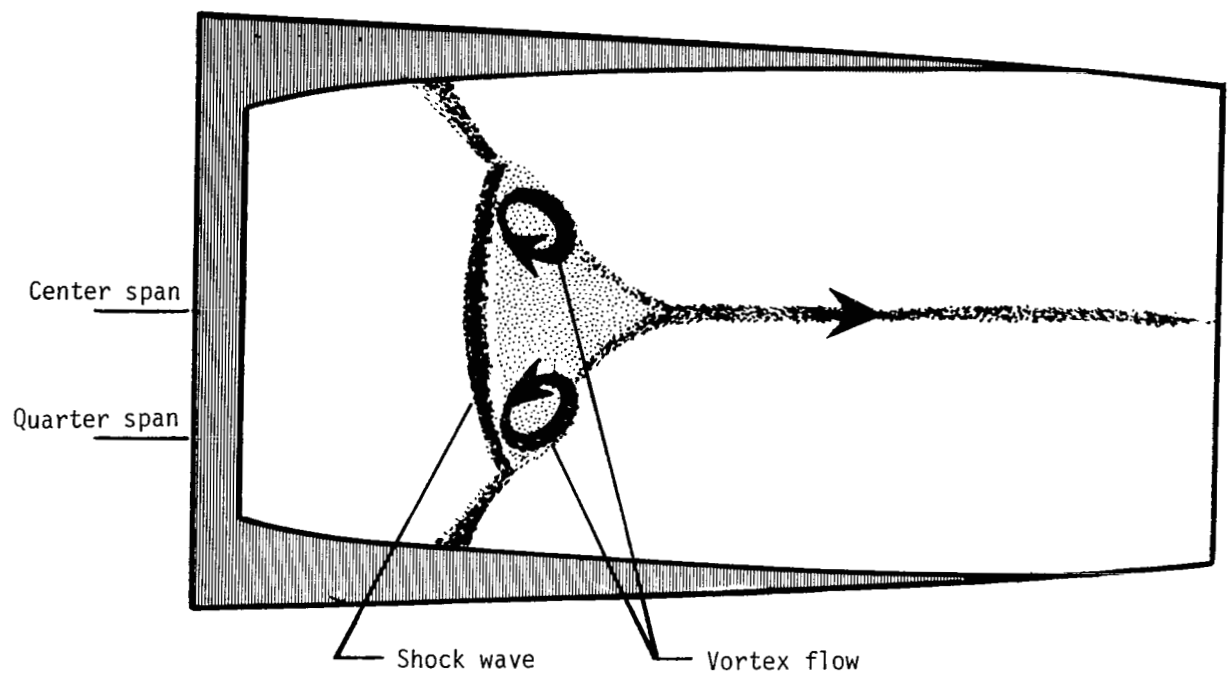
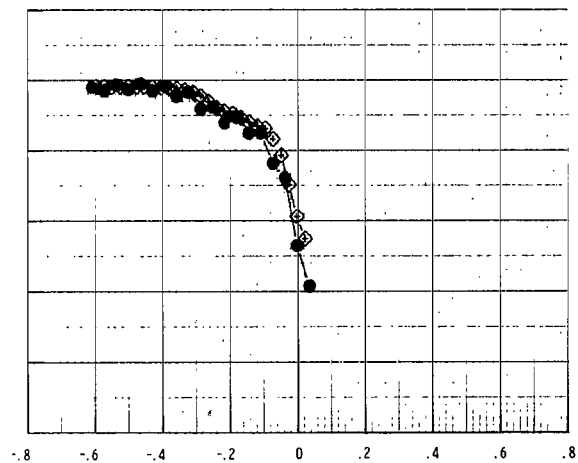
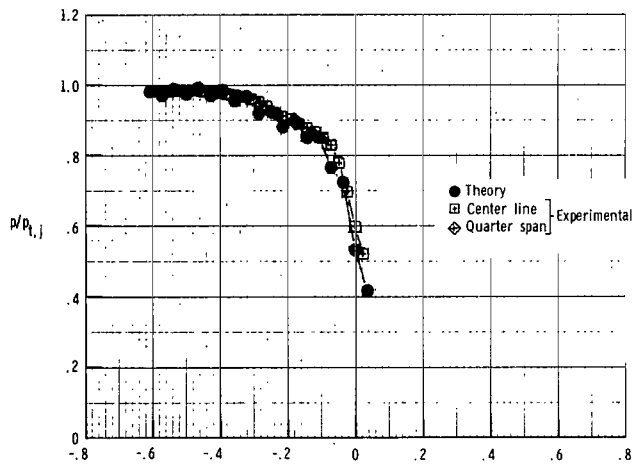
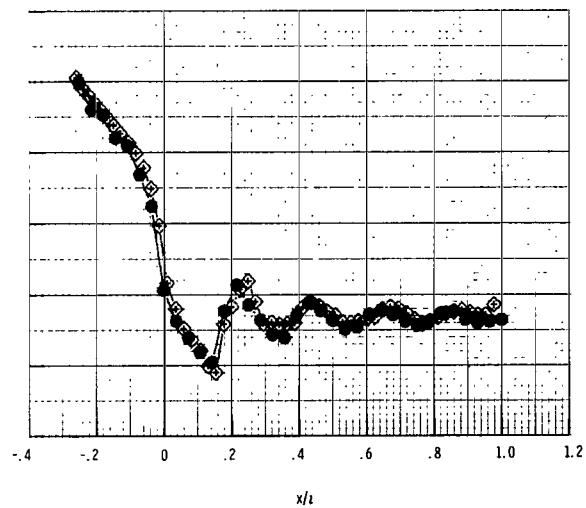
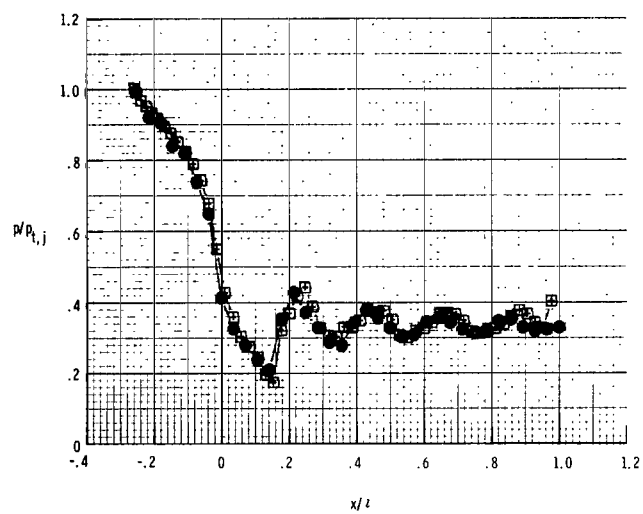


Figure 6.- Oil flow pattern. $p_{t,i}/p_a = 6.0$.

Cowl top



Wedge



(a) $p_{t,j}/p_a = 3.0$.

Figure 7.- Comparison of pressure distributions.

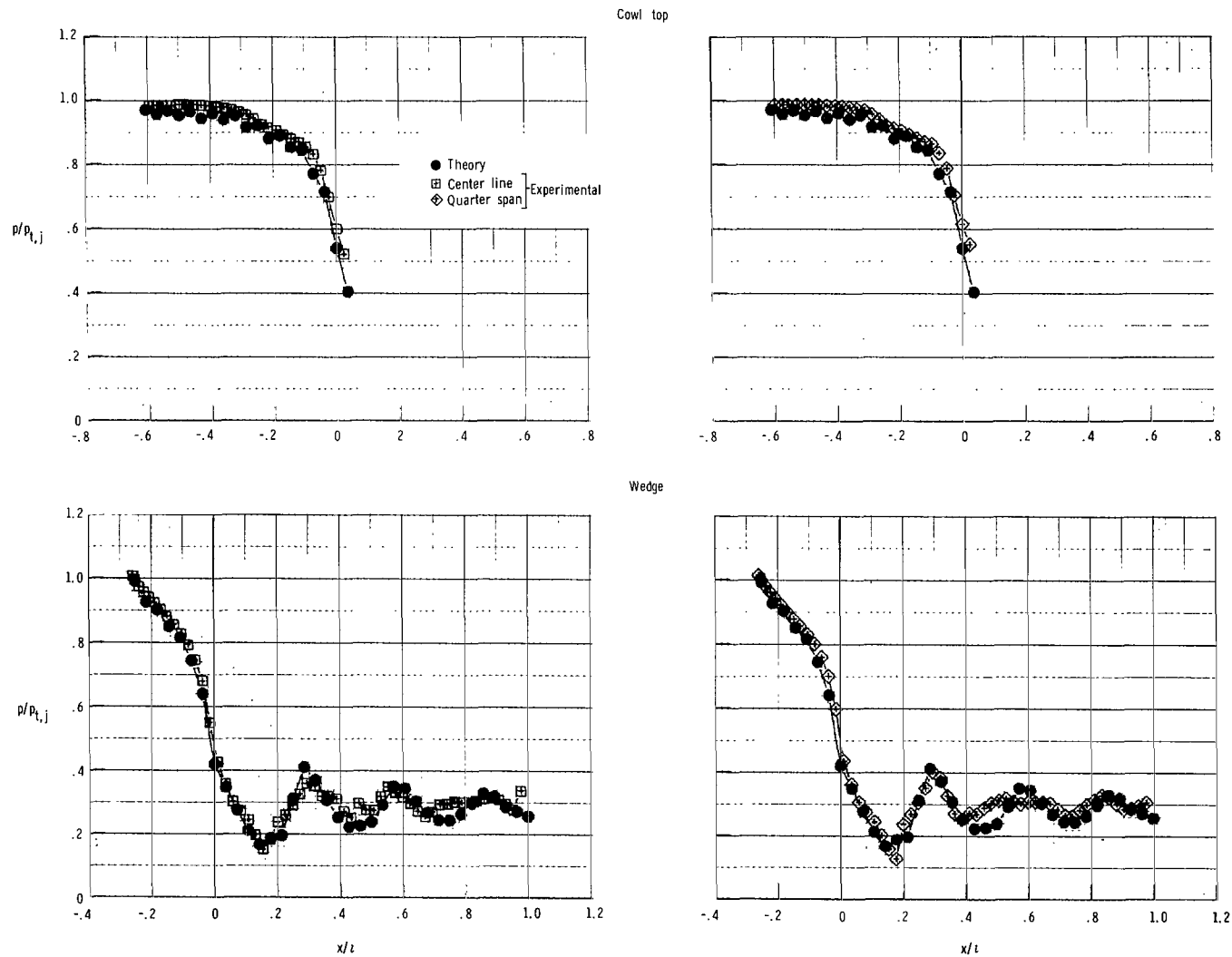
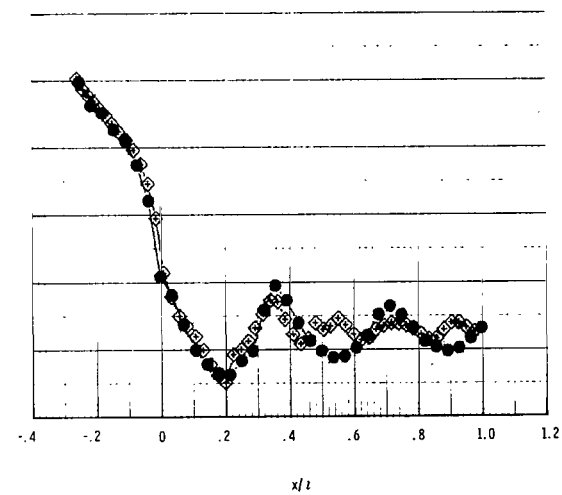
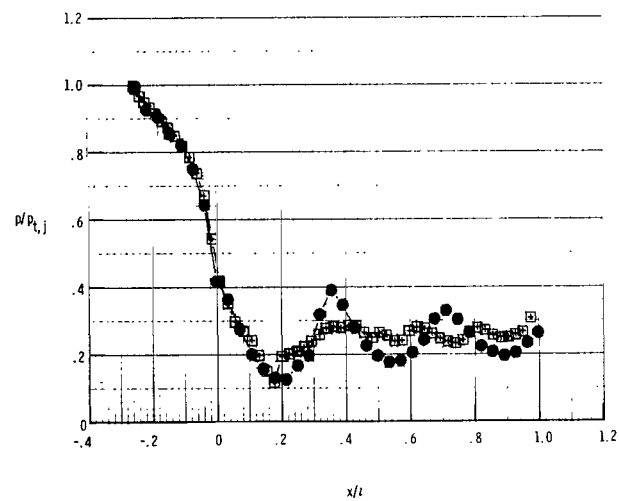
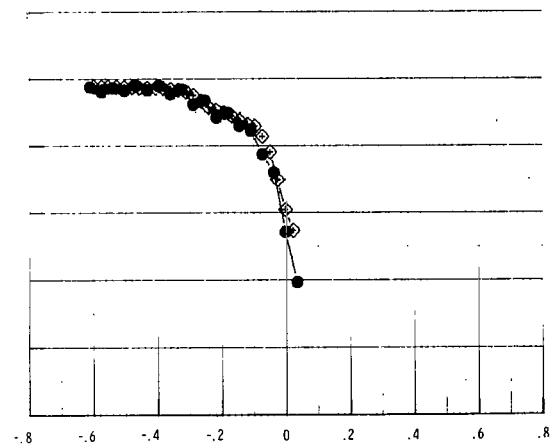
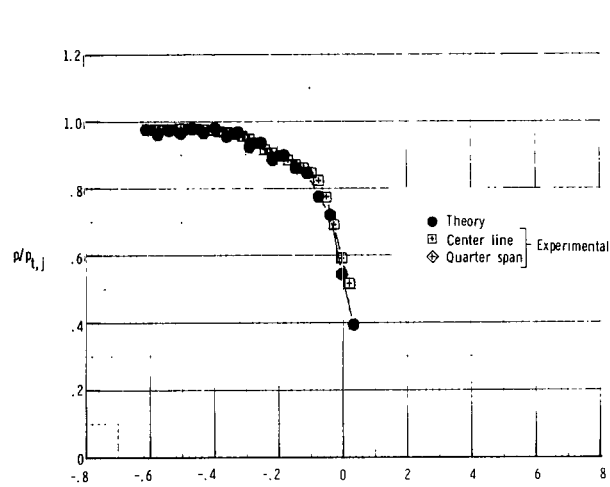


Figure 7.- Continued.



(c) $p_{t,j}/p_a = 4.0.$

Figure 7.- Continued.

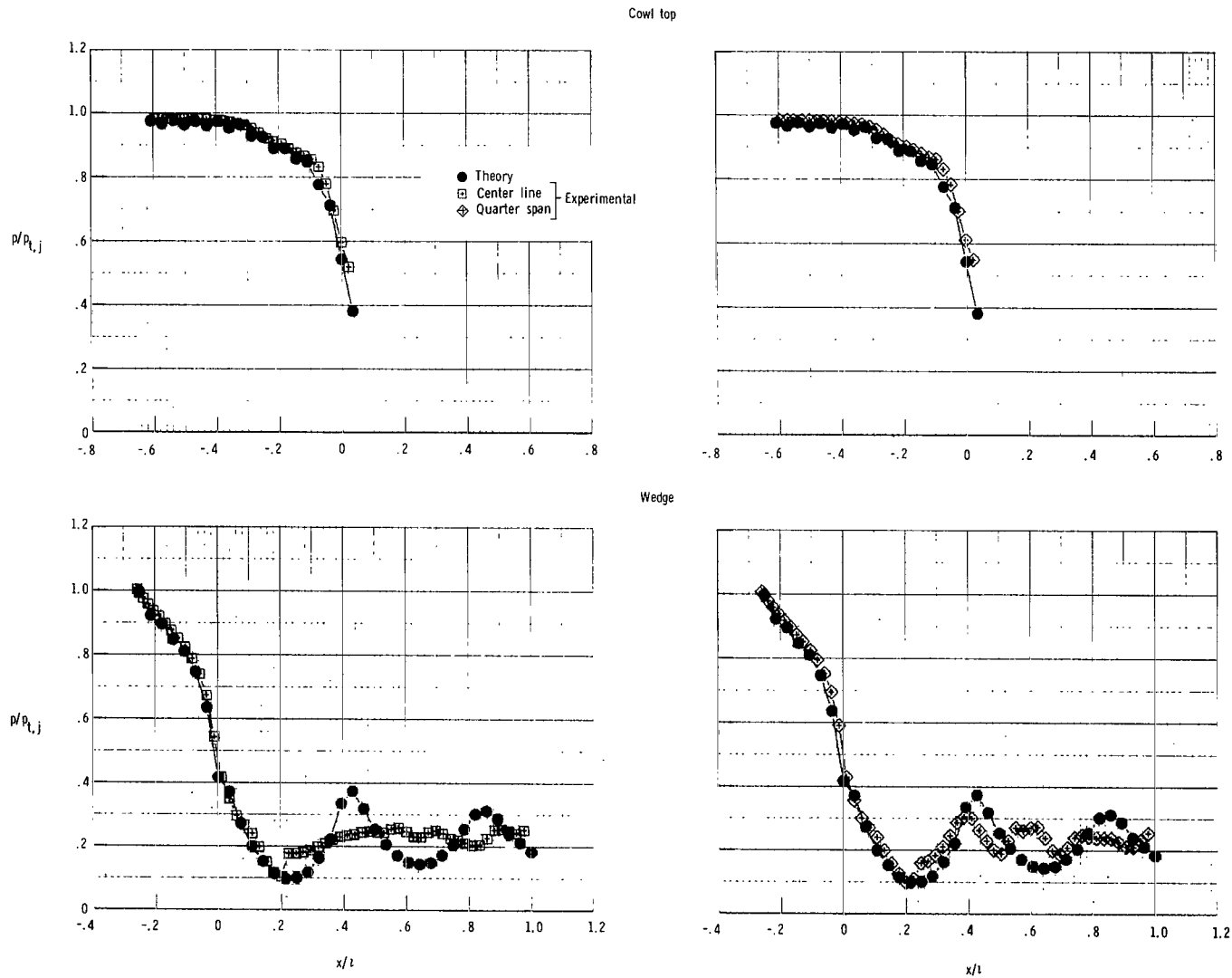
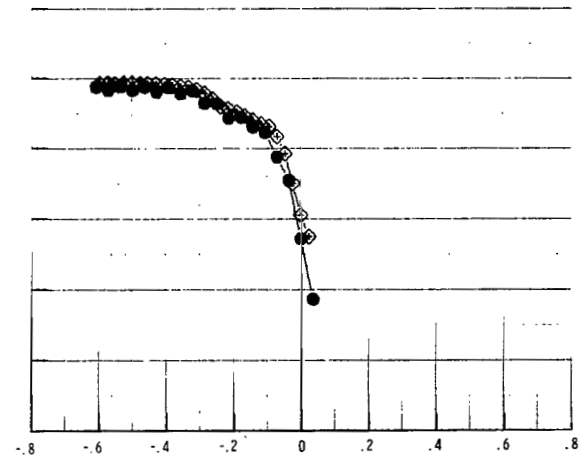
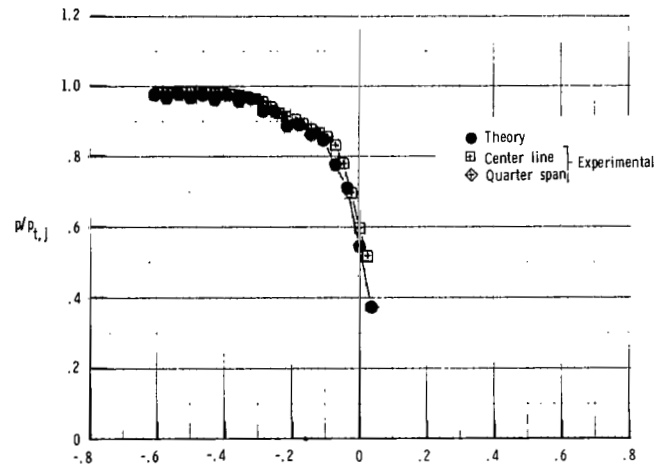
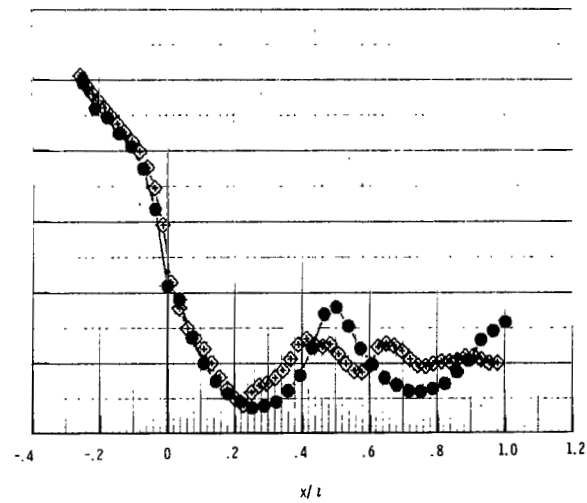
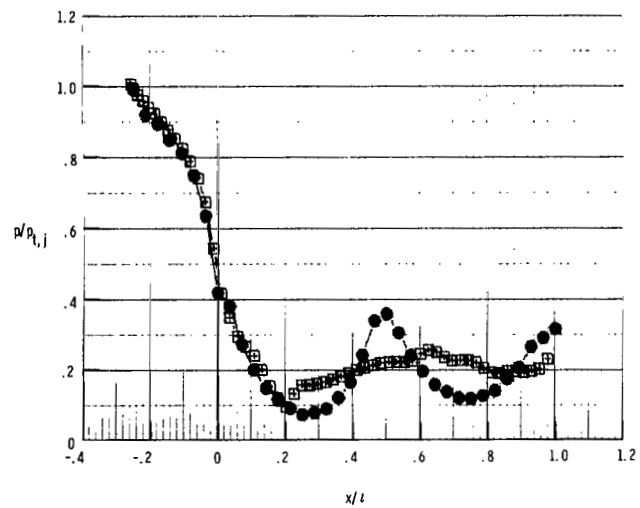


Figure 7.- Continued.

Cowl top



Wedge



(e) $p_{t,j}/p_a = 5.0$.

Figure 7.- Continued.

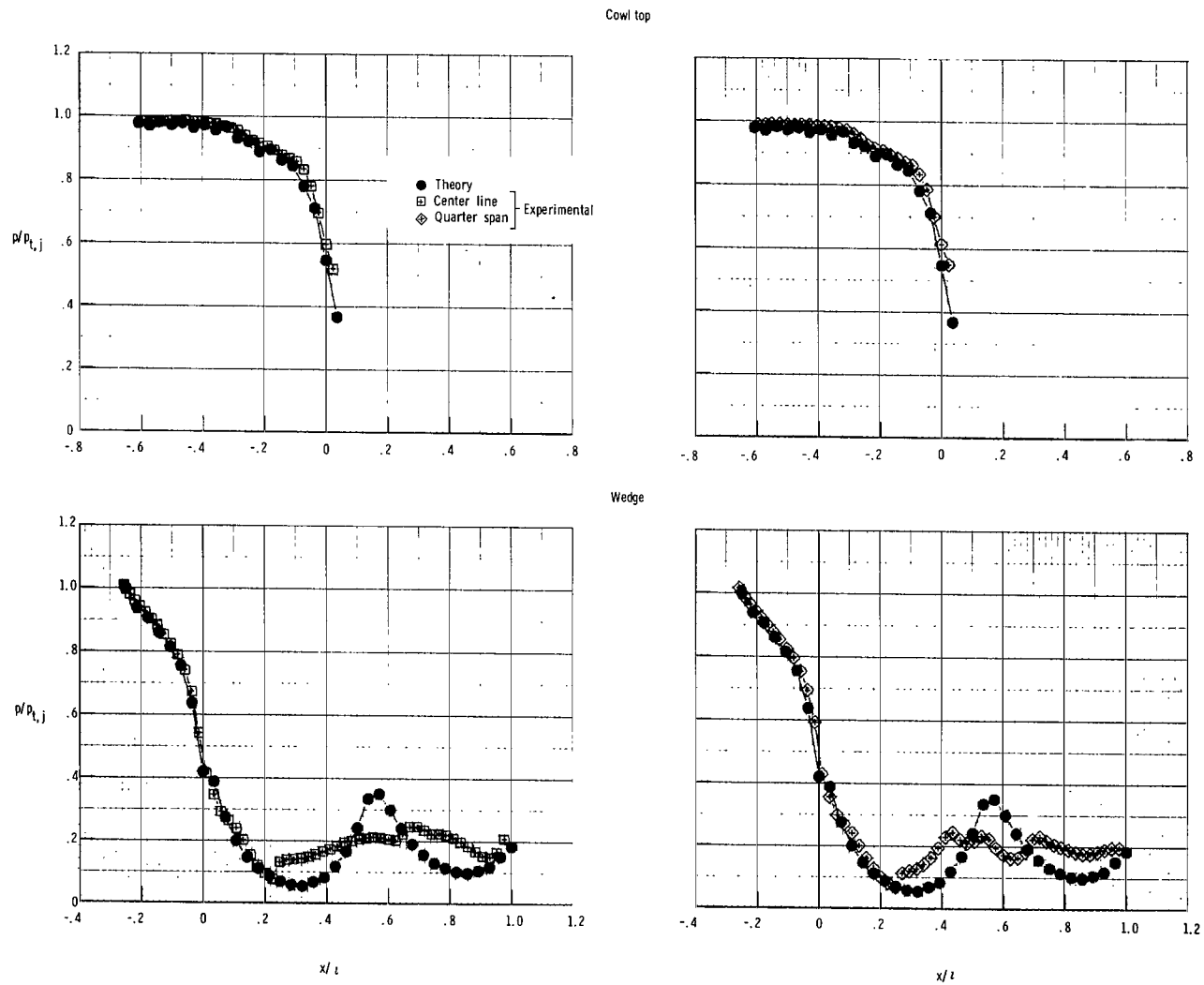
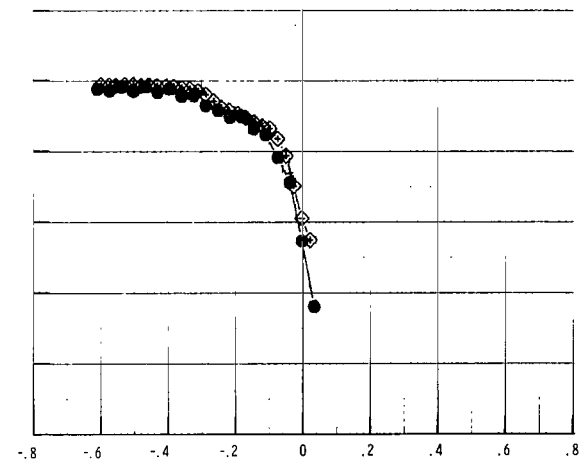
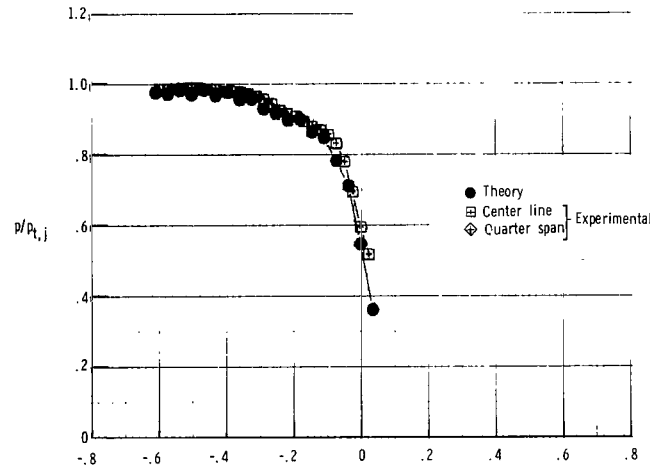
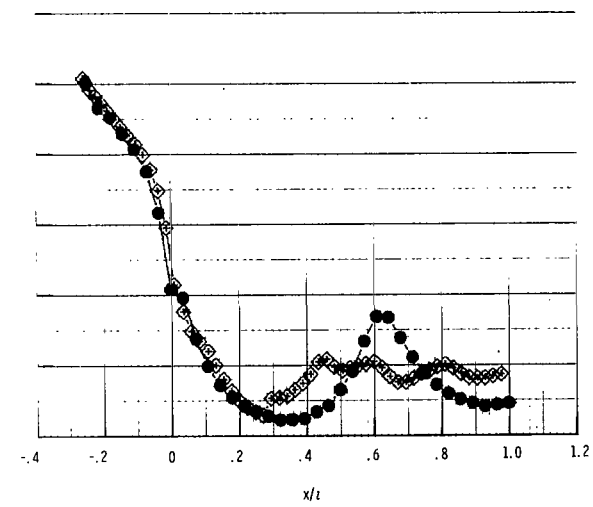
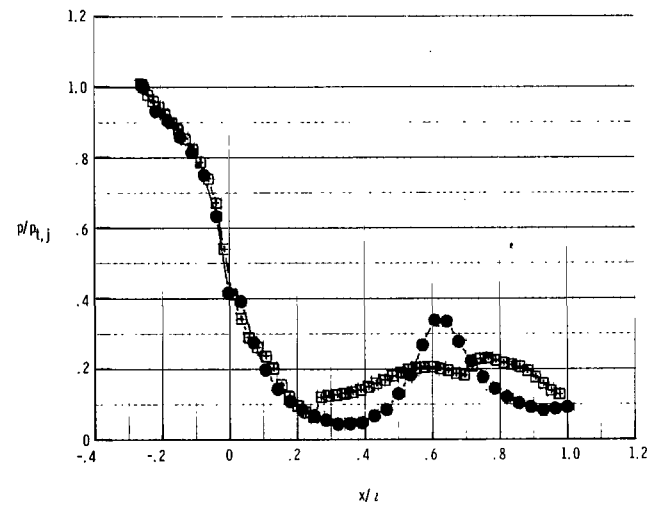


Figure 7.- Continued.

Cowl top



Wedge



$$(g) \quad p_{t,j}/p_a = 6.0.$$

Figure 7.- Concluded.

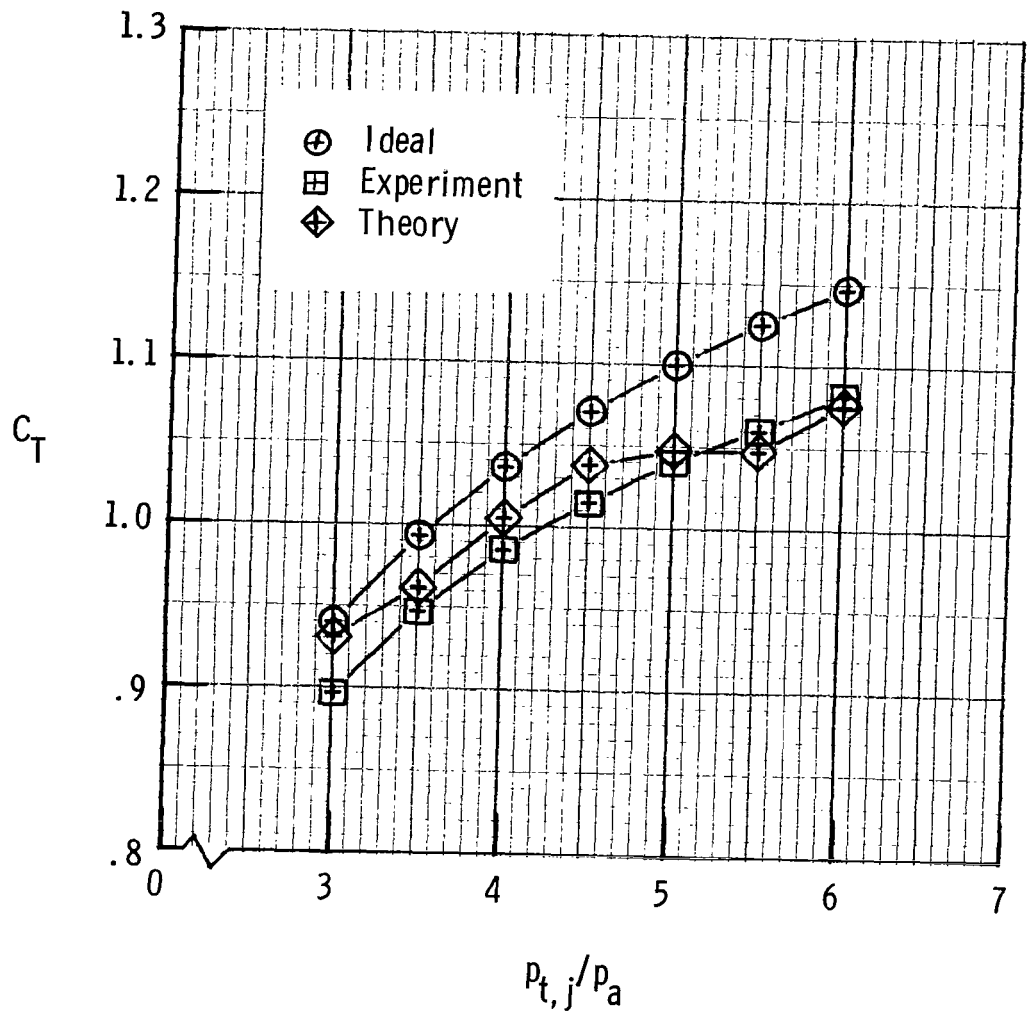


Figure 8.- Comparison of thrust coefficients.

1. Report No. NASA TP-1188	2. Government Accession No.	3. Recipient's Catalog No.	
4. Title and Subtitle EXPERIMENTAL AND ANALYTICAL INVESTIGATION OF A NONAXISYMMETRIC WEDGE NOZZLE AT STATIC CONDITIONS		5. Report Date July 1978	
		6. Performing Organization Code	
7. Author(s) George T. Carson, Jr., and Mary L. Mason		8. Performing Organization Report No. L-12065	
		10. Work Unit No. 505-11-23-06	
9. Performing Organization Name and Address NASA Langley Research Center Hampton, VA 23665		11. Contract or Grant No.	
		13. Type of Report and Period Covered Technical Paper	
12. Sponsoring Agency Name and Address National Aeronautics and Space Administration Washington, DC 20546		14. Sponsoring Agency Code	
15. Supplementary Notes			
16. Abstract An experimental investigation of a nonaxisymmetric wedge nozzle has been conducted at static conditions. The resulting data, in the form of detailed pressure distributions and oil flow photographs, expand the current nonaxisymmetric nozzle data base. An analytical investigation has been conducted to evaluate a two-dimensional, inviscid, time-dependent theory as a nonaxisymmetric nozzle performance predictor. For the range of nozzle pressure ratios investigated, results indicate good agreement between theory and experiment in regions of predominately two-dimensional flow and limited agreement in regions of three-dimensional flow. For the wedge nozzle and related nozzle configurations, the two-dimensional, inviscid theory may be applied as a limited performance predictor.			
17. Key Words (Suggested by Author(s)) Propulsion nozzles Nonaxisymmetric wedge nozzle NAP		18. Distribution Statement Unclassified - Unlimited Subject Category 02	
19. Security Classif. (of this report) Unclassified	20. Security Classif. (of this page) Unclassified	21. No. of Pages 42	22. Price* \$4.50

* For sale by the National Technical Information Service, Springfield, Virginia 22161

NASA-Langley, 1978

National Aeronautics and
Space Administration

Washington, D.C.
20546

Official Business

Penalty for Private Use, \$300

THIRD-CLASS BULK RATE

Postage and Fees Paid
National Aeronautics and
Space Administration
NASA-451



2 1 10, A, 060978 S00903DS
DEPT OF THE AIR FORCE
AF WEAPONS LABORATORY
ATTN: TECHNICAL LIBRARY (SUL)
KIRTLAND AFB NM 87117

NASA

POSTMASTER:

If Undeliverable (Section 158
Postal Manual) Do Not Return

S